



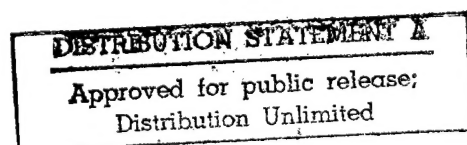
FOREIGN
BROADCAST
INFORMATION
SERVICE

JPRS Report

Science & Technology

***Central Eurasia:
Materials Science***

DITC QUALITY INSPECTED 2



19980116 194

Science & Technology

Central Eurasia: Materials Science

JPRS-UMS-92-012

CONTENTS

12 August 1992

Analysis, Testing

Intelligent Systems for Estimating and Forecasting Machine Service Life [Yu. N. Drozdov, G. K. Sorokin, et al.; Minsk TRENIYA I IZNOS, Vol 13 No 1, Jan 92]	1
Superelasticity and 'Shape Memory' Characteristics in Sintered Porous Titanium Nickelide [N. V. Goncharuk, I. F. Martynova, et al.; Kiev POROSHKOVAYA METALLURGIYA, No 4, Apr 92] ..	1
Strength Characteristics of Joints Made by Soldering Sphalerite and Wurtzite Modifications of Boron Nitride and Tested for Tensile and Shear Strength [Yu. V. Naydich, A. M. Martirosyan, et al.; Kiev POROSHKOVAYA METALLURGIYA, No 4, Apr 92]	1
Co-TiC _{0.86} -NbC _{0.9} Section of a Phase Equilibrium Diagram for the Co-Ti-Nb-C System [G. P. Dmitriyeva, T. S. Cherepova, et al.; Kiev POROSHKOVAYA METALLURGIYA, No 4, Apr 92] ..	2
Isotopic Exchange of Molecular Oxygen With La _{0.7} Sr _{0.3} CoO _{3-δ} Oxygen [G. K. Vdovin, B. L. Kuzin, et al.; Moscow POVERKHNOST: FIZIKA, KHIMIYA, MEKHANIKA, No 10, Oct 92]	2
Calculating Thermal Desorption Spectra for Hydrogen Implanted During Ion Bombardment [A. A. Pisarev and V. V. Kulik; Moscow POVERKHNOST: FIZIKA, KHIMIYA, MEKHANIKA, No 10, Oct 92]	2
Using Low-Energy Ion Scattering and Recoil Atoms To Analyze the Surface Structure of GaAs(100) [A. A. Aristarkhova, S. S. Volkov, et al.; Moscow POVERKHNOST: FIZIKA, KHIMIYA, MEKHANIKA, No 10, Oct 92]	3
Studying the Emissive Properties and Elemental Composition of Cesium-Implanted Niobium Single Crystals [V. I. Podgronyy, S. A. Zaslavskiy, et al.; Moscow POVERKHNOST: FIZIKA, KHIMIYA, MEKHANIKA, No 10, Oct 92]	3
Kinetics of the Interaction Between Oxygen and a Surface. Formation and Growth of the Oxide Phase on a Metal Surface [Yu. N. Devyatko, S. V. Rogozhkin, et al.; Moscow POVERKHNOST: FIZIKA, KHIMIYA, MEKHANIKA, No 10, Oct 92]	3
Phase Transformation Regularities Occuring During the Diffusion Saturation of Niobium With Both Silicon and Titanium [M. S. Tsirlin, S. U. Rybakov, et al.; Moscow POVERKHNOST: FIZIKA, KHIMIYA, MEKHANIKA, No 10, Oct 92]	4
Ionometric Determination of Na, K, NH ₄ , Ca, NO ₃ ⁻ , Cl ⁻ Ions in Sr, Ca, and V Compounds [L.V. Kvyatkovskaya, M.M. Mansurov, et al.; ZAVODSKAYA LABORATORIYA, No 2, Feb 92]	4
Mass-Spectrometry of Vinyl-Substituted Organoboron Compounds [V.O. Tarielashvili, K.G. Ordzhonikidze, et al.; ZAVODSKAYA LABORATORIYA, No 2, Feb 92]	5
Acoustic Method of Nondestructive Quality Control of Carbon Products [A.F. Grebenkin, I.B. Moskovenko; ZAVODSKAYA LABORATORIYA, No 2, Feb 92]	5
Nondestructive Inspection of Decarburized Cutting Tool [V.I. Bochenin; ZAVODSKAYA LABORATORIYA, No 2, Feb 92]	5
Group Concentration and Determination of Mn, Fe, Zn, Cu, Pb in Drainage-Tank Waters by Atomic-Absorption Analysis [N.N. Basargin, Yu.G. Rozovskiy, et al.; ZAVODSKAYA LABORATORIYA, No 3, Mar 92]	6
Extractive-Photometric Determination of Bi in Tinning Electrolyte [L.I. Toropov, M.I. Degtev; ZAVODSKAYA LABORATORIYA, No 3, Mar 92]	6
Determination of Wetting Angle Between Carbon Fiber Surface and Thermoplastic Melt [T.T. Sorina, Ye.Yu. Filippova; ZAVODSKAYA LABORATORIYA, No 3, Mar 92]	6
Effect of Chaotically Distributed Dislocations Density on Ti Diffusion in Mo Single Crystals [N.V. Dubovitskaya, L.D. Kolenchenko, et al.; METALLOFIZIKA, Vol 14 No 1, Jan 92]	7
On Structure of Intermediate Layers Forming During Explosive Interaction of Al With Steel [G.M. Grigorenko, V.V. Statsenko; METALLOFIZIKA, Vol 14 No 1, Jan 92]	7
Effect of Ferro- and Antiferromagnetic Critical Fluctuations on Frozen State Formation Mechanism in FeNiMn Alloys [Yu.P. Grebenyuk, G.A. Takzey; METALLOFIZIKA, Vol 14 No 1, Jan 92]	7

Structure of Surface Layers Forming Under Water-Cooled Nickel-Steel and Cobalt-Steel Pair Friction [O.N. Razumov, Yu.F. Shavadskiy; METALLOFIZIKA, Vol 14 No 1, Jan 92]	8
Effect of Annealing on Local Structure of Fe _{85-x} Co _x B ₁₅ Amorphous Alloys After γ -Irradiation [V.V. Polotnyuk, A.M. Shalayev, et al.; METALLOFIZIKA, Vol 14 No 1, Jan 92]	8
Structure Behavior of Rapidly Quenched Metal-Metalloid Alloys Under Exposure to Certain External Factors [G.M. Zelinskaya, L.Ye. Mikhaylova, et al.; METALLOFIZIKA, Vol 14 No 1, Jan 92]	8
Structural Factors Which Determine Reactor Graphite's Young Modulus Behavior After Irradiation and Annealing [I.Ya. Levintovich, A.S. Kotosonov, et al.; FIZIKA I KHIMIYA OBRABOTKI MATERIALOV, No 3, May-Jun 92]	9
Assessing Optical Properties of Glass Materials Modified in Plasma Discharge by Infrared Spectroscopy [M.K. Rodionov, N.P. Yevtushenko, et al.; FIZIKA I KHIMIYA OBRABOTKI MATERIALOV, No 3, May-Jun 92]	9

Coatings

'Third-Body' Formation and a Positive Mechanical Property Gradient Resulting From the Chemomechanical Application of a Brass Coating [G. Poltsier, A. Firkovskiy, et al.; Minsk TRENIYE I IZNOS, Vol 13 No 1, Jan 92]	10
Model of Coating Interaction That Accounts for Deformability, Wear, and Heat Liberation [V. M. Aleksandrov and G. K. Annakulova; Minsk TRENIYE I IZNOS, Vol 13 No 1, Jan 92]	10
Crystallization and Magnetic Properties of Co-P-Re Amorphous Electrolytically Precipitated Films [M.U. Sheleg, L.V. Nemtsevich, et al.; METALLOFIZIKA, Vol 14 No 1, Jan 92]	10
Plasma Spraying of ZrO ₂ -Based Sealing Coats [S.T. Televnyy, V.S. Yesenbekov, et al.; FIZIKA I KHIMIYA OBRABOTKI MATERIALOV, No 3, May-Jun 92]	11
Corrosion-Resistant Aluminide-Class Diffusion Coats on High-Temperature Alloys [A.A. Kopylov, O.V. Dvoretskyi, et al.; FIZIKA I KHIMIYA OBRABOTKI MATERIALOV, No 3, May-Jun 92]	11
Production of Powders Reinforced With Silicon Carbide Discrete Particles and Filamentary Crystals [I.Ye. Kalashnikov, V.N. Meshcheryakov, et al.; FIZIKA I KHIMIYA OBRABOTKI MATERIALOV, No 3, May-Jun 92]	11

Composite Materials

Matrix Synthesis—A New Method of Polymeric Low-Friction Composite Materials [I. A. Gribova, G. I. Gureyeva, et al.; Minsk TRENIYE I IZNOS, Vol 13 No 1, Jan 92]	13
--------------------------------------------------------------------------------------------------------------------------------------------------------------------	----

Corrosion

Improving the Corrosion-Resistance of Chromized Parts Made From Iron Powder [I. S. Litmanovich and Ya. M. Zolotovitskiy; Kiev POROSHKOVAYA METALLURGIYA, No 4, Apr 92]	14
Protective Coatings for Niobium, Tantalum, Molybdenum, and Tungsten To Increase Resistance to High-Temperature Oxidation [Yu. V. Dzyadykovich; Kiev POROSHKOVAYA METALLURGIYA, No 4, Apr 92]	14

Nonferrous Metals, Alloys, Brazes, Solders

Implantation of Nitrogen Together With Carbon or Oxygen in Molybdenum [Kh. R. Kazdayev, Ye. M. Bayadilov, et al.; Moscow POVERKHНОST: FIZIKA, KHIMIYA, MEKHANIKA, No 10, Oct 92]	15
Low-Temperature Diffusion of Platinum in Thin Copper Films [A. N. Aleshin, V. K. Yegorov, et al.; Moscow POVERKHНОST: FIZIKA, KHIMIYA, MEKHANIKA, No 10, Oct 92]	15

Nonmetallic Materials

Using Cement Plant Electrostatic Precipitator Dust in Glassmaking [N. I. Minko and K. I. Yermolenko; Moscow STEKLO I KERAMIKA, No 3, Mar 92]	16
-------------------------------------------------------------------------------------------------------------------------------------------------	----

Selecting Process Duration and Temperature When Molding Glassware From Sheet Glass [A. G. Shabanov, N. V. Lalykin, et al.; Moscow STEKLO I KERAMIKA, No 3, Mar 92]	16
Producing Photochromic Glass From a Synthetic Charge [A. B. Atkarskaya, O. I. Mironenko, et al.; Moscow STEKLO I KERAMIKA, No 3, Mar 92]	16
Outlook for Powder-Process Glass Ceramics [V. I. Solovyev, Ye. S. Akhlestin, et al.; Moscow STEKLO I KERAMIKA, No 3, Mar 92]	16
Optical Constants of Bismuth Containing Ga Glasses [A. I. Rabukhin and G. V. Belousov; Moscow STEKLO I KERAMIKA, No 3, Mar 92]	17
Fractal Properties of Interfaces in Zirconium Dioxide Powders Produced Using Plasma Chemistry Processes [Yu. Abzayev, N. V. Dedov, et al.; Moscow STEKLO I KERAMIKA, No 3, Mar 92]	17
Phase Transformations When Firing Ceramic Tiles Made Primarily of Ore-Dressing Gangue [V. Z. Abdrahimov; Moscow STEKLO I KERAMIKA, No 3, Mar 92]	17
Increasing the Stability of Enamel Slips for Composite Coatings [L. A. Kurakevich, I. V. Stefanyuk, et al.; Moscow STEKLO I KERAMIKA, No 3, Mar 92]	17
Relaxation Properties of Enamel Slips [A. V. Nikitenko; Moscow STEKLO I KERAMIKA, No 3, Mar 92]	18
Factors Affecting the Formation of Solid Solutions in Strontium-Barium Glass Ceramics [N. M. Bobkova and L. M. Silich; Moscow STEKLO I KERAMIKA, No 2, Feb 92]	18
Absorption by Pigments in FK-14 Glass [A. B. Atkarskaya, V. I. Borulko, et al.; Moscow STEKLO I KERAMIKA, No 2, Feb 92]	18
Densely Sintered and Porous Glass Ceramic Dielectrics [V. I. Solovyev, V. A. Leshina, et al.; Moscow STEKLO I KERAMIKA, No 2, Feb 92]	19
Alumino-Silicate Ceramic With BaO-CaO-SiO ₂ System Eutectic Additive [G. A. Afonina, V. G. Leonov, et al.; Moscow STEKLO I KERAMIKA, No 2, Feb 92]	19
Mechanism of Surface Layer Formation When Grinding and Sharpening Ceramics [V. S. Fadeyev; Moscow STEKLO I KERAMIKA, No 2, Feb 92]	19
Robot Arm for Applying Powdered Enamels [N. D. Parshin; Moscow STEKLO I KERAMIKA, No 2, Feb 92]	20
Polymer Coating for Ceramic Tile [D. N. Aneli, L. G. Shamanauri, et al.; Moscow STEKLO I KERAMIKA, No 2, Feb 92]	20
Study of Nb-Y ₂ O ₃ System Powder Component Interaction [A. Ye. Soloyeva; OGNEUPORY, No 6, Jun 92]	20
Measurement of ZrO ₂ -Based Ceramics Static Modulus of Elasticity [Ye.I. Akselrod, R. Ye. Vol'son; OGNEUPORY, No 6, Jun 92]	21
Heat Insulating Rubber for Dry Binder Grinding Ball Mill Lining [N.M. Shevchenko, G.P. Sheludko, et al.; OGNEUPORY, No 6, Jun 92]	21
Dolomite-Dunite Mixture as Fettling Material for Steelmaking Furnaces [G.I. Antonov, V.P. Nedosvityi, et al.; OGNEUPORY, No 6, Jun 92]	21
Structure and Phase Composition of Rammed Lining and Channel Fouling Products of Magnetodynamic Aluminum Alloy Meters [A.V. Kosinskaya, Zh.D. Bogatyreva; OGNEUPORY, No 6, Jun 92]	22

Preparations

Numerical Modeling of Powder Compacting Utilizing an Axisymmetrical Impact [V. A. Gorelskiy and S. A. Zelepugin; Kiev POROSHKOVAYA METALLURGIYA, No 4, Apr 92]	23
Use of Hydrostatic Pressure of up to Five GPa To Compact Tungsten Powders of Various Dispersity [V. P. Filonenko, L. G. Khvostantsev, et al.; Kiev POROSHKOVAYA METALLURGIYA, No 4, Apr 92]	23
Studying the Sintering Process in the I ₂ O ₃ -CuO System [Yu. I. Boyko, Yu. I. Klinchuk, et al.; Kiev POROSHKOVAYA METALLURGIYA, No 4, Apr 92]	23
Hot-Pressed Cupreous Powder Steels [S. G. Napara-Volgina; Kiev POROSHKOVAYA METALLURGIYA, No 4, Apr 92]	23
Optimizing the Composition of the Nickel Binder in WC-Ni Hard Alloys by Alloying the Binder With Elements From Groups IV-VI [R. F. Cheburayeva, I. N. Chaporova, et al.; Kiev POROSHKOVAYA METALLURGIYA, No 4, Apr 92]	24
Shrinkage and Dimensional Accuracy in Products Made of Sintered Titanium Alloy [V. N. Kazakov, V. I. Kryukov, et al.; Kiev POROSHKOVAYA METALLURGIYA, No 4, Apr 92]	24
Generation of Vacancies Stimulated by the Chemical Etching of a Crystal Surface [A. G. Italyantsev; Moscow POVERKHnost': FIZIKA, KHIMIYA, MEKHANIKA, No 10, Oct 92]	25

High-Vacuum Thermal Cleaning of Si Surfaces With a Protective Oxide Film <i>[V. A. Perevoshchikov, V. D. Skupov, et al.; Moscow POVERKHНОСТ: FIZIKA, KHIMIYA, MEKHANIKA, No 10, Oct 92]</i>	25
------------------------------------------------------------------------------------------------------------------------------------------------------------------------------------------------------	----

Treatments

α -Ti Straining Temperature Manipulation. Mechanical and Substructural Aspects <i>[A.R. Smirnov, V.A. Moskalenko; METALLOFIZIKA, Vol 14 No 1, Jan 92]</i>	26
Effect of Dynamic Straining on Steel 30KhN4M Microstructure Kinetics <i>[S.A. Atroshenko, S.A. Gladyshev, et al.; METALLOFIZIKA, Vol 14 No 1, Jan 92]</i>	26
Microcrack Curing in Pulse Strained Mo During Annealing <i>[M.N. Belyakova, Yu.V. Konyushin, et al.; METALLOFIZIKA, Vol 14 No 1, Jan 92]</i>	26
Characteristics of Fe and Ni Mass Transfer in Metals During Propagation of Pulse Radiation-Generated Shock Waves <i>[A. Dubik, L.O. Zvorykin, et al.; METALLOFIZIKA, Vol 14 No 1, Jan 92]</i>	27
Effect of Proton Irradiation on Electric Charge Formation in Mailar and Teflon Films <i>[V.V. Gromov, G.M. Sessler, et al.; FIZIKA I KHIMIYA OBRABOTKI MATERIALOV, No 3, May-Jun 92]</i>	27
High-Dose Fe Ion Implantation at Room Temperature <i>[E.M. Diasamidze, A.N. Kalinin; FIZIKA I KHIMIYA OBRABOTKI MATERIALOV, No 3, May-Jun 92]</i>	27
Age-Harden Nickel Alloy Behavior Under Radiative Heat Treatment <i>[N.M. Zaytseva, I.I. Volodina, et al.; FIZIKA I KHIMIYA OBRABOTKI MATERIALOV, No 3, May-Jun 92]</i>	27
Phase Formation in V_2O_5 Single Crystals Under Irradiation With Electrons of Varying Energy <i>[L.M. Kryukova, Ye.V. Uspenskaya; FIZIKA I KHIMIYA OBRABOTKI MATERIALOV, No 3, May-Jun 92]</i>	28
Effect of Pulse Laser Radiation on Wrought Aluminum Alloys <i>[S.A. Maslyayev, V.I. Neverov, et al.; FIZIKA I KHIMIYA OBRABOTKI MATERIALOV, No 3, May-Jun 92]</i>	28
Structural Changes in Encapsulated Polysilicon Layers Under Effect of Scanning Laser Radiation <i>[A.A. Druzhinin, I.T. Kogut, et al.; FIZIKA I KHIMIYA OBRABOTKI MATERIALOV, No 3, May-Jun 92]</i>	28
Effect of Laser Radiation on CdTe Optical and Mechanical Properties <i>[A.V. Savitskiy, P.P. Beysyuk, et al.; FIZIKA I KHIMIYA OBRABOTKI MATERIALOV, No 3, May-Jun 92]</i>	29
Simulation of Cosmic Radiation Effect on Materials <i>[A.I. Akishin, I.B. Teplov (deceased); FIZIKA I KHIMIYA OBRABOTKI MATERIALOV, No 3, May-Jun 92]</i>	29
Effect of Polishing on Surface Properties of Glass <i>[N.N. Khomenko, S.Yu. Lysenko; FIZIKA I KHIMIYA OBRABOTKI MATERIALOV, No 3, May-Jun 92]</i>	29

Welding, Brazing, Soldering

Explosion Welding of Tubes to Tube Plates <i>[Yu.L. Alekseyev, L.I. Lepekhina, et al.; FIZIKA I KHIMIYA OBRABOTKI MATERIALOV, No 3, May-Jun 92]</i>	31
--------------------------------------------------------------------------------------------------------------------------------------------------------------	----

Extractive Metallurgy, Mining

Alekseyevka Deposit Dolomites <i>[T.N. Dolgikh, A.K. Karklit, et al.; OGNEUPORY, No 6, Jun 92]</i>	32
Analysis of Chalganovskiy Deposit Kaolin <i>[R.S. Shulyak, V.V. Primachenko, et al.; OGNEUPORY, No 6, Jun 92]</i>	32
Statute on Procedure for Mineral Licensing <i>[KOMMERSANT, No 29, 13-20 Jul 92]</i>	32

Miscellaneous

Thermostable Magnets of Hysteretic Motor System <i>[Ye.V. Belozerov, N.M. Kleynerman, et al.; FIZIKA METALLOV I METALLOVEDENIYE, No 10, Oct 91]</i>	35
Effect of Magnetized Water on Dough Properties and Bread Quality <i>[A.M. Ostapenkov, I.M. Mamatov, et al.; ELEKTRONNAYA OBRABOTKA MATERIALOV, No 5 (161), Sep-Oct 91]</i>	35

Intelligent Systems for Estimating and Forecasting Machine Service Life

927D0136B Minsk TRENIA I IZNOS in Russian
Vol 13 No 1, Jan 92 pp 122-129

[Article by Yu. N. Drozdov, G. K. Sorokin, and D. Ya. Stadnikov, Institute of Machine Science imeni Academician A. A. Blagonravov at the USSR Academy of Science, Moscow; UDC 621.891]

[Abstract] A model of a PC-based intelligent system for analyzing tribological problems is described. All of the hardware and software requirements of such a system are detailed, as are the analytical functions that such a system should be able to perform. The model in question is based largely on a multi-level frame model of friction and wear that is designed for the tribological analysis of IC engine cylinder liners and upper compression rings. Computer applications of this model are discussed. The authors feel that their approach to the design and construction of intelligent systems could be effectively utilized to develop other types of intelligent systems for use by engineering research and design personnel. Figures 4; references 9: 7 Russian, 2 Western.

Superelasticity and 'Shape Memory' Characteristics in Sintered Porous Titanium Nickelide

927D0177H Kiev POROSHKOVA METALLURGIYA in Russian No 4, Apr 92 pp 56-59

[Article by N. V. Goncharuk, I. F. Martynova, O. R. Naydenova, V. V. Skorokhod, S. M. Solonin, and G. R. Fridman, Institute of Applied Materials Science of the Ukrainian Academy of Sciences, Kiev; UDC 621.762:5.001:539.4.42:620.18]

[Abstract] Superelasticity and shape memory were studied in sintered titanium nickelide. Cylindrical specimens 10 mm in diameter with an h/d ratio of approximately 1 were compacted from PN56T44 powder and sintered in a $6.65/10^{-3}$ Pa vacuum for one hour. Porosity after sintering was 50 and 43 percent. To obtain specimens with 30 percent porosity, the specimens were twice-compacted and sintered. The specimens were cyclically upset on an Instron testing machine that recorded the load diagram. Curves of the direct/reversible deformation and direct deformation/shape recovery relationships showed that, as porosity increased, the curves became flatter, with their maximums shifting towards the higher direct deformation values. The maximum values for reversible deformation also increased as porosity increased. Conversely, as porosity decreases, the degree of shape recovery as a function of direct deformation drops more abruptly. The nature of these relationships was attributed to the concurrence of two factors: an increase in the volume and degree of martensitic deformation of the solid phase, and an increase in the volumetric proportion and degree of deformation of material undergoing deformation due to

conventional plastic flow mechanisms. Analogous relationships were established between these shape memory characteristics and the interrelationships of porosity, upsetting load, and number of loading cycles. When cyclically loaded specimens were gradually heated to 400°C, it was found that the interplay of porosity and load also affected reversible deformation. It was also found that, given a specific porosity, the contribution of shape recovery to complete reversible deformation declines as upsetting load increases. Figures 5, tables 1; references 6: Russian.

Strength Characteristics of Joints Made by Soldering Sphalerite and Wurtzite Modifications of Boron Nitride and Tested for Tensile and Shear Strength

927D0177I Kiev POROSHKOVA METALLURGIYA in Russian No 4, Apr 92 pp 60-66

[Article by Yu. V. Naydich, A. M. Martirosyan, and G. A. Kolesnichenko, Institute of Applied Materials Science of the Ukrainian Academy of Sciences, Kiev; UDC 621.762:620.179:621.791:661.55:620.191]

[Abstract] Joints made by soldering polycrystals of sphalerite and wurtzite modifications of boron nitride—elboron-P and hexanite-P—to metal were tested to determine tensile and shear strength and the nature of joint failure. The materials were soldered in a .002-.005-Pa vacuum at 850-1000°C using copper and silver-based solders with 4 wt. percent titanium. The tensile-test specimens were made by soldering cylindrical polycrystals end-to-end to steel pins, using a specially designed device to keep the two components aligned. The shear-test specimens were made by soldering polycrystals face-to-face to rectangular steel plates. The tensile tests were performed on an RM-0.5 tester at room temperature and a deformation rate of 6 mm/min, and the shear tests on special equipment. The huge disparity in strength values and the application of Weibull's modulus to these data revealed that the strength of the soldered joints is largely determined by the strength of the polycrystals, which in turn depends on structural characteristics such as homogeneity, grain size, and various types of imperfections. As these characteristics are greatly affected by soldering conditions, joint strength itself depends on soldering temperature, duration, and so forth. Optimal soldering temperature and duration were found to be 850°C and 3-7 min., respectively. Higher soldering temperatures and/or longer soldering times result in diffusion processes that adversely affect the formation of new boride and nitride phases that create a solid bond between the solder and the polycrystal. Other factors affecting the nature of joint strength are the steel's coefficient of linear expansion and the location of the rupture surface. Figures 6, tables 1; references 20: 19 Russian, 1 Western.

Co-TiC_{0.86}-NbC_{0.9} Section of a Phase Equilibrium Diagram for the Co-Ti-Nb-C System

927D0177J Kiev POROSHKOVAYA METALLURGIYA in Russian No 4, Apr 92 pp 78-82

[Article by G. P. Dmitriyeva, T. S. Cherepova, and A. K. Shurin, Institute of Physical Metallurgy of the Ukrainian Academy of Sciences, Kiev; UDC 669.017.13.25'293'295'784]

[Abstract] A phase equilibrium diagram of the Co-Ti-Nb-C quaternary system was constructed, and the Co-TiC_{0.86}-NbC_{0.9} section of this diagram used to study alloys of this system. A permanent tungsten electrode was used to fuse the alloys in a laboratory electric-arc furnace equipped with a water-cooled copper hearth. The charge consisted of pure metals: titanium iodide, electron-beam melted niobium, electrolytic cobalt, and spectrally pure graphite. Fusion took place in an argon atmosphere. As the castings solidified, they were cooled at a rate of 20 degrees/sec. Metallographic, differential thermal, and X-ray phase analysis were used to study the alloys in their as-cast state and after vacuum annealing at 1000°C for 0.5 hours, 1200° for 20 hours, and 1300°C for 48 hours. The data showed that the section has one monovariant eutectic transformation with a temperature that smoothly decreases from the fusion temperature of the Co-NbC eutectic to that of the Co-TiC eutectic. The melting temperature of the alloys ranges from 10-15 degrees along the line representing monovariant eutectic crystallization. Annealing does not appreciably affect alloy fusion temperature. In the cast state, all of the alloys contain a solid solution of two cobalt modifications—hexagonal and cubic; the lattice spacing is virtually identical in all cases. Section alloys annealed at 1300°C and cooled along with the furnace contained mostly a solid solution based on the hexagonal cobalt modification. The only carbide phase found in the section was a solid solution of TiC and NbC single carbides with an NaCl-type crystal lattice, which inherently has a non-equilibrium state during solidification at a rate of 10-20 degrees/second. Figures 4; tables 1; references 10: 7 Russian, 3 Western.

Isotopic Exchange of Molecular Oxygen With La_{0.7}Sr_{0.3}CoO_{3-δ} Oxygen

927D0182A Moscow POVERKHНОST: FIZIKA, KHIMIYA, MEKHANIKA in Russian No 10, Oct 92 pp 30-35

[Article by G. K. Vdovin, B. L. Kuzin, and E. Kh. Kurumchin, Institute of Electrochemistry of the Ukrainian Division of the USSR Academy of Sciences, Sverdlovsk; UDC 541.128.13+541.135.5+541.183.5]

[Abstract] An isotopic exchange method was used to measure the exchange rate of O₂ with La_{0.7}Sr_{0.3}CoO_{3-δ} in a specially modified static circulation apparatus. The specimens were either in powder form or in the form of a densely sintered bar 3.1 x 3.1 x 13.6 mm in size. Typical curves representing the relationship between

temperature and the heteroexchange rate for the sintered specimens show that the rate declines as temperature increases. The slope of the curve is roughly 45°, and the curve shifts to the right and up when pressure is increased from 1.6 to 10 torr. A typical curve has both a high- and a low-temperature section, and the temperature of transition from the former to the latter increases by about 30° when pressure is increased from 1.6 to 10 torr. The points representing the transitions from the high- to low-temperature regions were attributed to the appearance of Co²⁺ ions acting as new exchange reaction centers on specimen surfaces at elevated temperatures. The curve for the powder specimens is much lower and further to the right and has an unbroken slope. The heteroexchange rate gradually increases as pressure is increased, but lower temperatures result in a downward shift of the pressure vs. exchange rate curve. The activation energies associated with the sintered specimens were: 205 + 41, T = 1251 - 1127, 10 torr; 82 + 16, T = 1077 - 906, 10 torr; 185 + 41, T = 1179 - 1102, 5 torr; 70 + 17, T = 1047 - 941, 5 torr; 213 + 72, T = 1157 - 1121, 1.6 torr; 77 + 12, T = 1083 - 1001, 1.6 torr. For the powder specimens, activation energy was 123 + 8 and 119 + 15, with T = 743 - 634 and 694 - 624, and pressure 10 and 5 torr, respectively. Figures 4, tables 1; references 17: 13 Western, 4 Russian.

Calculating Thermal Desorption Spectra for Hydrogen Implanted During Ion Bombardment

927D0182B Moscow POVERKHНОST: FIZIKA, KHIMIYA, MEKHANIKA in Russian No 10, Oct 92 pp 41-48

[Article by A. A. Pisarev and V. V. Kulik, Moscow Institute of Engineering Physics; UDC 533.924]

[Abstract] A mathematical model was used to calculate the thermal desorption spectra of hydrogen while varying the ion implantation parameters. The curves representing thermal desorption spectra transformation as a function of ion fluence, defect production rate, and binding energy showed a series of gassing peaks, most of which were approximately symmetrical, shifting to the higher temperature regions. This shift was attributed mainly to a higher ion fluence, but peak symmetry was also tied to high defect production rates and moderate binding energies, regardless of placement. The temperature of the maximum as a function of binding energy and defect production rate showed an approximately linear increase when binding energy was greater than 0.3 eV and the defect production rate greater than five, but at lower values for these parameters, it tended to be more representative of defect-free diffusion. Peak width ($\Delta T_1/2$) varied non-monotonically with binding energy, the defect rate, and, hence, with the temperature of the maximum. Peak position was found to depend on the ratio of binding energy to diffusion activation energy given a constant energy at which hydrogen is released from a defect. The lower the diffusion activation energy, the faster the diffusion process, and the later the manifestation of the gassing peak. Deterioration in surface

permeability results in a radical transformation of the thermal desorption spectra that is attributed to restricted gassing induced by the thermal desorption from the surface. The model of diffusion gassing yields a broader thermal diffusion spectrum and is more comprehensive than other models. However, the undefined parameter allowing arbitrariness in the calculation of binding energy is the defect concentration. Depending on the conditions, gassing can be restricted by liberation from defects, diffusion, or desorption. Figures 7; references 6: 5 Western, 1 Russian.

Using Low-Energy Ion Scattering and Recoil Atoms To Analyze the Surface Structure of GaAs(100)

927D0182C Moscow POVERKHНОST: FIZIKA, KHIMIYA, MEKHANIKA in Russian No 10, Oct 92 pp 90-95

[Article by A. A. Aristarkhova, S. S. Volkov, V. V. Trukhin, and G. N. Shuppe, Scientific Research Institute of Technology, Ryazan; UDC 537.534:539.211]

[Abstract] The potential of using low-energy back-scattered ions and recoil atoms at the same time to study the surface structure of GaAs(100) was assessed. The experiments were performed on a single-crystal GaAs(100) n-type wafer that was ion-bombarded and annealed at 870 K. Ne⁺ ions (3 keV of energy) served as the primary ions. The angular distributions of the scattered Ne⁺ ions and the Ga⁺ recoil atoms were measured and recorded on an energy-analyzing apparatus similar to a 180-degree spherical deflector (energy resolution 0.5 percent) mounted on a tilting platform that permitted varying the scattering angle from 0 to 130°. The specimen manipulator made it possible to vary the glancing angle from 0 to and the azimuth angle of the specimen position up to 200° from its original direction. Residual gas pressure in the pressure chamber was 2(10⁻¹⁰) torr. The glancing angle was set at 130° when analyzing the energy distribution of the scattered ions and at 60° when analyzing the ionized recoil atoms. To minimize ion-induced surface damage, a defocused beam ($d = \text{approximately } 3-4 \text{ mm}$) was used. The spectra were recorded within narrow energy bands corresponding to the position of the peaks of the basic elements. The results showed that the angular distributions of low-energy scattered ions and recoil atoms can be used to perform elemental and structural analysis of complex surfaces. The angular distribution data obtained from the experiments were reconciled with a computer model of these data, and the reconciled data were used to construct a complex four-level experimental model of the surface structure of GaAs(100)-c(8.2). This model is based on surface As-dimers constituting 0.25 of the monomolecular film and on Ga-dimers arranged in the lowest gallium layer. Figures 4; references 12: 9 Western, 3 Russian.

Studying the Emissive Properties and Elemental Composition of Cesium-Implanted Niobium Single Crystals

927D0182D Moscow POVERKHНОST: FIZIKA, KHIMIYA, MEKHANIKA in Russian No 10, Oct 92 pp 117-121

[Article by V. I. Podgornyy, S. A. Zaslavskiy, and R. C. Chilingarashvili; UDC 537.58]

[Abstract] The emissive properties and elemental composition of cesium-doped niobium single crystals were studied on electropolished and vacuum-annealed wafers cut parallel to the crystal face (110) to a 0.003-m thickness. Cs⁺ ions with 20 keV of energy were implanted at room temperature at a dose rate of 10¹⁹ m⁻². One of the specimens was also irradiated by O⁺ ions with the same energy level at a dose rate of 10²⁰ m⁻². The specimens were slowly heated to 1300-1400 K in an ultimate vacuum of 10⁻⁶ Pa, and, as the temperature was gradually decreased in 40-50° intervals, the volt-ampere characteristics of an experimental diode-type apparatus with an interelectrode spacing of 0.001 m were measured. Specimen temperature was measured with a W-Re thermocouple. The effect that holding the specimens at a constant temperature in the electric field of the anode has on emission current was studied, as was the behavior of the emission current after the specimens were heated. Auger electron spectroscopy was used to study the elemental surface composition of the specimens during the heating process. The results of the experiment showed that there is a strong relationship between the work function of cesium doped- niobium and temperature, with the work function decreasing after ion implantation and heating. This relationship was attributed to the formation on the specimen surface of a layer of dipoles of adsorbed cesium that had migrated from deep inside the specimen during the heating process and to the formation in the near-surface region of a chemical compound containing alloying elements perhaps akin to niobium bronze and characterized by a low work function. The rise and fall of specimen emission current under both types of heating conditions could be explained by a change in Cs concentration in the near-surface region of a specimen. Figures 3; references 12: 10 Russian, 2 Western.

Kinetics of the Interaction Between Oxygen and a Surface. Formation and Growth of the Oxide Phase on a Metal Surface

927D0182F Moscow POVERKHНОST: FIZIKA, KHIMIYA, MEKHANIKA in Russian No 10, Oct 92 pp 129-131

[Article by Yu. N. Devyatko, S. V. Rogozhkin, V. N. Tronin, and V. I. Troyan, Moscow Institute of Engineering Physics; UDC 536.76.539]

[Abstract] Oxide growth in the form of islets on a metal surface and the kinetics of oxygen-surface interaction

near the Curie point of magnetic materials are investigated and represented mathematically. The growth of the oxide phase is described within the framework of the phenomenological theory of phase transformations. Oxide formation on a metal surface is a first-order phase transition consisting of two stages: the supply of oxygen to the growing oxide islet, and the direct transformation of the particles approaching the nucleus into a new phase. The oxygen reaches the growing islet directly from the gaseous phase at the islet perimeter or as a result of adsorbed oxygen flowing to the islet. Islet growth is a random process and can be described by a Fokker-Planck-type equation that can be used to calculate the extent to which a surface is filled by large isolated islets. This relationship between time and a wide range of values for the extent to which a surface is filled with islets was observed when oxidizing nickel. The non-trivial relationship between the nickel oxidation rate and temperature arises naturally within the phenomenological framework in the case of finite phase transformation times. The kinetics of oxygen-surface interaction near the Curie point of magnetic materials is characterized by a number of anomalies. To describe these processes, it is necessary to account for the interaction between adatoms effected through the magnetic subsystem, which in turn determine the growth rate of the oxide phase islets and the extent to which they cover a particular surface. References 14: 8 Russian, 6 Western.

Phase Transformation Regularities Occuring During the Diffusion Saturation of Niobium With Both Silicon and Titanium

927D0182G Moscow *POVERKHnost: FIZIKA, KHIMIYA, MEKHANIKA* in Russian No 10, Oct 92 pp 132-137

[Article by M. S. Tsirlin, S. Yu. Rybakov, and G. M. Anurova, Institute of Physical Chemistry of the USSR Academy of Sciences, Moscow; UDC 621.793:669.293]

[Abstract] The use of powder metallurgy to induce the diffusion saturation of niobium with both titanium and silicon was investigated. Specimens of 99.96 percent pure Nb in the form of wire 2 mm in diameter and 50-60 mm long and wafers 10 x 10 x 1 cu mm, were simultaneously titanized and siliconized in a mixture of Ti and Si powders that contained dry Ca, Mg, and K fluoride additives in an amount equal to 3 percent of total composition mass. The powder mixture was prepared in such a way as to obviate Ti-Si interaction during the diffusion process. Diffusion saturation was carried out in a 10^{-3} -Pa vacuum at 1373-1573 K. Elemental and phase compositions of the coatings, which formed during the interaction of the niobium with a gaseous phase containing silicon and titanium fluorides, were inspected on a Camebax spectroscope and a DRON-3 diffractometer (CuK α -radiation). Coating structure was studied with the aid of an optical and scanning electron microscope. It was found that coating phase composition is dictated by the thermodynamic activity of the components of the particular powder mixture used for diffusion saturation.

The best results were achieved when diffusion was carried out for two hours at 1573 K, as this ensured a noticeable transfer of Ti into the coating. Different formulations of the diffusion compositions resulted in different concentrations of silicon and titanium in the coating. Coating thickness varied from 4 to 36 μ m. In Ti-rich mixtures, titanizing predominated (15-57 percent Ti), and Si concentration did not exceed 0.5 percent in the Nb-Ti solid solution zone. When Si concentration in the mixtures equalled 26 percent, coating thickness and Ti concentration were minimal (4 μ m and 0.1 percent, respectively). With higher Si concentrations, Ti concentration at first increased to 15 percent, then steadily dropped off to 3-4 percent. Figures 4, tables 2; references 4: 3 Russian, 1 Western.

Ionometric Determination of Na,K,NH₄,Ca,NO₃⁻, Cl⁻ Ions in Sr, Ca, and V Compounds

927D0184A Moscow ZAVODSKAYA LABORATORIYA in Russian No 2, Feb 91 (manuscript received 24 Apr 91) pp 10-11

[Article by L.V. Kvyatkowskaya, M.M. Mansurov, G.L. Semenova, A.N. Pugovenko, M.M. Usmanova, Z.U. Sokhibov, and G.F. Fayezov, Tajik University imeni V.I. Lenin, Dushanbe; UDC 543.257.1]

[Abstract] An ionometric determination of Na,K,NH₄,Ca,NO₃⁻,Cl⁻ impurity ions in Ca, Sr, and V compounds was made by the method of standard additions, using commercially available appropriate ion-selective electrodes. The e.m.f. of galvanic cells was measured in an I-115 ionometer with an EVL-1 M3 AgCl reference electrode and with a saturated KCl or NH₄NO₃ solution filling the salt bridge. In this way was made a quantitative determination of those impurity ions in analytical specimens of Ca₂V₂O₇ (for special alloys), V₂O₅ (for special alloys), SrCO₃ (1. for lumino-phors, 2. granulated for radioelectronic apparatus), SrHPO₄ (for luminophors), SrCrO₄ (for graphic arts, pigment, rust-resistant primer), Sr(NO₃)₂ (pure and analytically pure grades). The readings indicated that the concentration of each impurity ion in each compound was well within the acceptable range. The readings were, moreover, reproducible with a sufficiently high precision allowing an evaluation of the pA dependence of the e.m.f. (pA—concentration index, A= Na⁺, K⁺, NH₄⁺, Ca²⁺, NO₃⁻, Cl⁻) for calibration of the electrode function. The latter was found to be linear for each of the ion-selective electrodes. The very close agreement between the impurity concentration readings obtained by this method and those obtained by other methods (photometry, flame photometry, nephelometry, complexonometry) suggests that this simple and fast method with excellent reproducibility of readings can be used in laboratory practice, its additional advantage being that the possibility of simultaneous quantitative determination of several different ions in the same specimen. The method is, accordingly, already used in the laboratory at Isfara Hydrometallurgical Plant. Tables 1; references 2.

Mass-Spectrometry of Vinyl-Substituted Organoboron Compounds

927D0184B Moscow ZAVODSKAYA LABORATORIYA
in Russian No 2, Feb 92 (manuscript 10 Sep 90)
pp 18-20

[Article by V.O. Tariyelashvili, K.G. Ordzhonikidze, L.P. Parulava, and G.V. Vakhaniya, Scientific Research Institute of Stable Isotopes, Tbilisi; UDC 543.51]

[Abstract] In connection with laser-chemical separation of boron isotopes in synthesized organoboron compounds with substitutions in the vinyl group, five such substances were analyzed in a mass-spectrometer: 1) 2-chloralkenyl dichloroborane, 2) 2-chloropropen-1-yl-dichloroborane, 3) 2-chloro-trans-butene-2-yl-3-dichloroborane, 4) 2-chlorobutene-2,2-dichloroborane, 5) 2-chlorostyrene-2-dichloroborane. The analysis was performed in an MI-1201 mass-spectrometer with electron-impact ionization, one advantage of this ionization method being that it combines high intensity of ionization with high stability of ion currents. Another advantage is a rather thorough fragmentation of a specimen, which makes it possible to detect functional groups as well as to determine both the stoichiometric and structure formulas of the compound. In the mass (m/e) spectrum of a specimen the peaks representing the given compound could not be readily identified at first, owing to the presence of impurity compounds in the specimen, but only after the impurities had been identified by comparing the mass spectrum of the end product of synthesis with those of the reactants and the intermediate products. The fragmentation of the five organoboron compounds was found to follow similar patterns, electron impact generating unstable molecular ions: 51 at. percent in 2-chloralkenyl dichloroborane and 0.2-4 at. percent in all the four others. Inasmuch as fragmentation involving detachment of hydrogen from the molecular ions was negligible throughout the 5-95 at. percent range of ^{10}B isotope concentration, this process was disregarded in calculation of the $^{10}\text{B} : ^{11}\text{B}$ ratio in those compounds. Figures 1; tables 1. references 1

Acoustic Method of Nondestructive Quality Control of Carbon Products

927D0184C Moscow ZAVODSKAYA LABORATORIYA
in Russian No 2, Feb 92 (manuscript received
23 Oct 90) pp 23-25

[Article by A.F. Grebenkin, All-Union Scientific Research and Design Institute of Aluminum, Magnesium, and Electrode Industry, I.B. Moskovenko, Scientific-Industrial Association for Abrasives and Grinding, St.Peterburg; UDC 620.179.16]

[Abstract] A method of nondestructive quality control has been developed for carbon products, namely an acoustic method and thus one which does not require cutting notches in the specimen. Only one parameter needs to be determined, the speed of sound (longitudinal

elastic waves) $c_i = (E/\rho)^{1/2}$ (E, ρ - modulus of normal elasticity and density of material) in a thin rod having been selected so that the spectrum of natural frequencies of such a specimen can be readily calculated on the basis of the $f_i = F_i c_i$ relation (F_i - coefficient depending on shape and size of inspection piece as well as on vibration mode). Conversely, from the measured natural frequencies one can calculate the speed of sound for a subsequent determination of physical and mechanical properties: apparent density, porosity, mechanical strength, and electrical resistivity. These properties, measurable by standard methods on special specimens, have been found to closely correlate with those acoustic characteristics of carbon products. The method was tested on many Soviet and foreign products such as graphitized electrodes, nipples, and plates for the chemical industry. The method has been subsequently refined by replacement of the speed of sound c_i with the "sound index" S.I.= $(c_{i, \min} + c_{i, \max})/200$ m/s. The apparatus for inspection by this method consists of amplifier stages, an automatic control system, a set of counters, an indicator panel, and stabilized power supplies. It has been put together with "Zvuk" (Sound) 107, 202, 203, and 203u components. Figures 1; references 3

Nondestructive Inspection of Decarburized Cutting Tool

927D0184D Moscow ZAVODSKAYA LABORATORIYA
in Russian No 2, Feb 92 (manuscript received 4 Oct 90)
pp 28-30

[Article by V.I. Bochenin, Kurgan Institute of Machine Design; UDC 620.179.5:531.75]

[Abstract] A method of nondestructive inspection has been developed for cutters made of high-speed tool steel, the carbon content in the surface layer being determined on the basis of density measurement after heat treatment as indicator of its martensite and austenite content. Inspection by the comparison method involves irradiating the surface of a test sample and that of a reference specimen with a collimated beam of γ -radiation and recording the also collimated characteristic K-radiation of tungsten, a key alloying element in these steels, the intensity of this radiation depending on the density in an inverse-law relation. This dependence can be made sufficiently strong and the inspection thus sufficiently sensitive by appropriately presetting either the angles α, β between the two collimators or the energy of primary radiation. The inspection is based on relative measurements in an experimental apparatus consisting of standard components: holder for the test sample, holder for the reference specimen, two sets of two collimators 8 mm in diameter, one for primary γ -radiation and one for secondary W-K radiation in each, two ^{57}Co -sources (123 keV and 10^8 Bq each), two scintillation detectors of secondary radiation, and a common 2-channel γ -spectrometer. Each detector is, together with the corresponding γ -radiation source, placed in common portable case so as to facilitate scanning the entire tool. The spectrum analyzer is tuned for maximum sensitivity of

Analysis, Testing

the signal to changes in the density of steel. The method and the apparatus were tested on 7 mm thick 60 mm square flat specimens of R-12 and R-6Mo5 tool steels after heat treatment at optimum respective temperatures. The reliability of the results was confirmed by chemical analysis of chips cut from surface layers of such specimens. Figures 2; tables 1; references 3.

Group Concentration and Determination of Mn, Fe, Zn, Cu, Pb in Drainage-Tank Waters by Atomic-Absorption Analysis

927D0185A Moscow ZAVODSKAYA
LABORATORIYA in Russian No 3, Mar 92
(manuscript received 25 Oct 90) pp 8-9

[Article by N.N. Basargin, Y.G. Rozovskiy, N.V. Chernova, and G. Radzhabov, Institute of Geology, Ore Deposits, Petrography, Mineralogy, and Geochemistry, Russian Academy of Sciences, Moscow; UDC 543.3.543.422]

[Abstract] A simple and fast method of group concentration and subsequent selective determination of Mn-II, Fe-III, Zn-II, Cu-II, Pb-II microquantities ($n \cdot 10^{-3}$ - $n \cdot 10$ percent) in drinking and drainage-tank water in Turkmenia is proposed, with poly(n)styrene-azo-yrocatechol serving as gelatinous sorbent. In the form of a dark-blue fine-disperse powder, this sorbent is insoluble in water, acids, bases, and organic solvents. Quantitative and selective group extraction of Mn, Fe, Zn, Cu, Pb takes place at a pH 6.5-7.0 in the presence of $n \cdot 10^6$ wt. excess Ti, Mo, W, SO_4^{2-} ; $n \cdot 10^5$ wt. excess K, Na, Mg; $n \cdot 10^4$ wt. excess Ca, F-, Cr-IV, HPO_4^{2-} ; $n \cdot 10^3$ wt. excess Li; $n \cdot 10^2$ wt. excess Cr-III. To a 500 ml sample of drinking or freshly tapped and filtered drainage-tank water are added first 3 ml of a 1:1 aqueous H_2SO_4 solution and then, for breaking the complexes in drainage-tank water, 0.5 g $(\text{NH}_4)_2\text{S}_2\text{O}_8$. An hour later excess acid is neutralized with NH_3 , whereupon is added as much CH_3COONa as necessary for the pH to fall within the 6.5-7.0 range and then 50 mg of the polymer sorbent after it has been passed through a "blue ribbon" filter. The concentrate is thoroughly washed with distilled water, whereupon Mn, Fe, Zn, Cu, Pb are desorbed from it with 1 M HCl solution, and the eluate is poured into a measuring tube. Final determination of those impurities is made by atomic-absorption flame spectrometry, although other techniques can be used for this, an oxyacetylene torch with three orifices and an AAS-1N "Karl Zeiss Jena" atomic-absorption spectrophotometer having been used for testing this method. Figures 1; tables 3; references 5

Extractive-Photometric Determination of Bi in Tinning Electrolyte

927D0185B Moscow ZAVODSKAYA LABORATORIYA
in Russian No 3, Mar 92 (manuscript received
16 Feb 90) pp 9-10

[Article by L.I. Toropov and M.I. Degtev, Perm State University imeni A.M. Gorkiy; UDC 546.87:54261:543.42.)62]

[Abstract] An experimental study was made concerning the feasibility of Bi-III extraction and complex formation with an antipyrine + thiourea derivative in the presence CCl_3COO^- ions, which would increase the sensitivity of extractive-photometric Bi-III determination in the presence of excess Fe (more than 18 times Bi), Cd (more than three times Bi), Pb (more than Bi), Cu (more than half Bi). A master solution of 0.1 M Bi-III was prepared by dissolving analytically pure $\text{Bi}(\text{NO}_3)_3 \cdot 5\text{H}_2\text{O}$. Working solutions of Bi-III were prepared by stepwise diluting the master with 0.2 M HNO_3 . These were used with solutions of pure CCl_3COO^- in distilled water and with chloroform-alcohol solutions of diantipyrine thiourea, the electronic absorption spectra being recorded with an SF-26 spectrophotometer and the infrared spectra being recorded with an IKS-29 spectrometer. Tests were performed on electrolytes consisting of 40-60 g/dm³ SnSO_4 + 100-110 g/dm³ H_2SO_4 + 0.8-1.5 g/dm³ $\text{Bi}_2(\text{SO}_4)_3$ + 0.3-0.8 g/dm³ NaCl + 4.5 g/dm³ preparation OS-20. The optical density of extracts was measured with a KFK-2MP photoelectric calorimeter using a light filter, chloroform solutions of diantipyrine thiourea being used for control tests. Diantipyrine thiourea was found to extract Bi-III from CCl_3COO^- solutions into chloroform in the form of a dyed compound (BiSO_4 maximally absorbing 365 nm light). On the basis of the test data has been established the dependence of not only Bi-III extraction level but also Pb++, Cu++, Fe++, Cd++, Zn++ extraction levels from their 0.01 M solutions on the CCl_3COO^- concentration, also the CCl_3COO^- concentration dependence of Bi-III macroquantity extraction (from 10⁻² M solutions) and microquantity extraction (from 2.5 x 10⁻⁵ M solution). The results indicate that the Bouguer-Lambert-Beer law is obeyed throughout the 0-1.1 mg/25 ml range. It takes about 20 minutes to complete one Bi-III determination. Figures 2; tables 1; references 9

Determination of Wetting Angle Between Carbon Fiber Surface and Thermoplastic Melt

927D0185C Moscow ZAVODSKAYA LABORATORIYA
in Russian No 3, Mar 92 pp 26-27

[Article by T.T. Sorina and Ye.Y. Filippova, Scientific-Industrial Association "All-Union Scientific Research Institute of Aviation Materials", Moscow]

[Abstract] A method of determining the wettability of carbon fibers by molten thermoplastic powder to serve as binder is proposed, essentially a variant of the sessile drop method based on change of the wetting angle. A solid powder grain of known size is deposited on a carbon monofilament, whereupon both are heated to the highest fluidization temperature of the thermoplastic material. The angle which a small droplet forms with the monofilament surface after it has spread over it at that temperature will serve as measure of binder's fiber wetting capacity, a smaller angle corresponding to a higher wetting capacity. The apparatus for such a determination consists of heater with a microthermal chamber, a frame for mounting the monofilament, a

micromanipulator, and a potentiometer with a rheostat. The angle readings are averaged over 10-15 measurements made on one batch of carbon fibers. The method was applied to polysulfone and polyester-ether.ketone, untreated or dressed, on ELUR-P and UKN-P carbon fibers. For carbon fibers, the wetting capacity of polysulfone was found to be lower (50-60° angle) than that of polyester-ether.ketone (29° angle). Figures 1; tables 1; references 3

Effect of Chaotically Distributed Dislocations Density on Ti Diffusion in Mo Single Crystals

927D0191A Kiev METALLOFIZIKA in Russian
Vol 14 No 1, Jan 92 pp 3-8

[Article by N.V. Dubovitskaya, L.D. Kolenchenko, L.N. Larikov, Physics of Metals Institute at the Ukrainian Academy of Sciences, Kiev; UDC 539.219.3:669.28]

[Abstract] The process of mass transfer in Mo single crystals exposed to low-energy Ti ion irradiation where the mass transfer mechanism is controlled on the surface by the radiation-stimulated volume diffusion (RSD) and in the bulk—by diffusion by the dislocation mechanism is discussed, and the lack of comprehensive published data on the effect of the dislocation density on the Ti mass transfer is noted. The Ti mass transfer process in (100) Mo single crystals with various dislocation densities during the titanium nitride coat application by low-energy plasma spraying is investigated. High purity Mo crystals are used in the study and thin wafers are sliced parallel to the (100) plane by electric cutting; the cold-worked layer is removed by electrochemical pickling. The samples are then rolled in the [100] direction and the dependence of the logarithmic Ti concentration on its penetration depth is plotted. The dislocation spacing distribution in strained Mo single crystals is examined and the hardness and angular blurring behavior of the Laue spot under the titanium nitride layer in Mo single crystals with varying degrees of straining are studied. The findings indicate that the dislocation density does not affect titanium's radiation-stimulated volume diffusion in Mo since ionic implantation generates a large number of point defects which is much stronger than the effect of the increase in the dislocation density; the chaotically distributed dislocation density does not affect the mass transfer by the dislocation mechanism. An increase in the mass transfer rate is observed only in the case where the existing surplus of dislocations of the same sign is sufficient to form new subboundaries in the crystal. The need to examine further the interaction of the newly formed dislocations generated during the mass transfer with the chaotically distributed dislocations created by pretreatment and its effect on the mass transfer is stressed. Figures 5; references 13: 5 Russian, 8 Western.

On Structure of Intermediate Layers Forming During Explosive Interaction of Al With Steel

927D0191E Kiev METALLOFIZIKA in Russian
Vol 14 No 1, Jan 92 pp 41-45

[Article by G.M. Grigorenko, V.V. Statsenko, Electric Welding Institute imeni Ye.O. Paton at the Ukrainian Academy of Sciences, Kiev; UDC 539.2]

[Abstract] The process of shock pulse interaction characterized by high degrees of plastic deformation of the near-contact layers, local heating, and a high mass transfer is discussed, and the structure of the intermediate layer forming in the joint of a three mm thick AD1 aluminum sheet with a 20 mm thick sheet of stainless steel 12Kh18N10T produced by explosion welding is examined by the transmission electron microscopy technique. The explosion cladding is performed by the parallel collision method at a 2,150 m/s detonation rate. An electron diffraction analysis demonstrates that the interaction process has a liquid phase origin with subsequent rapid melt quenching: An intensive Al interaction with stainless steel under explosion welding causes a joint melting of the surface layers of the colliding metals with subsequent rapid solidification of the thin melt layer while the material in the columnar formations developing in the layer after the explosion has a face-centered cubic lattice (GTsK) with a lattice parameter somewhat greater than that of pure Al. The high cooling rates attained during explosion cladding lead to the formation of an amorphous Al-Fe phase in the intermediate layer. Figures 4; tables 1; references 11: 8 Russian, 3 Western.

Effect of Ferro- and Antiferromagnetic Critical Fluctuations on Frozen State Formation Mechanism in FeNiMn Alloys

927D0191G Kiev METALLOFIZIKA in Russian
Vol 14 No 1, Jan 92 pp 74-81

[Article by Yu.P. Grebenyuk, G.A. Takzey, Physics of Metals Institute at the Ukrainian Academy of Sciences, Kiev; UDC 538.2:536.764:669.15]

[Abstract] The issue of the paramagnetic-spin glass (PM→SS) temperature transition and the fact that in concentrated alloys of the 3d-transition metals this transition may occur both at a fixed critical temperature and within a broad temperature range are discussed, and it is speculated that ferromagnetic (FM) and antiferromagnetic (AFM) orders may fluctuate and interact with each other, thus affecting the frozen state formation mechanism. To check this hypothesis, face centered cubic lattice FeNiMn alloys with various quasibinary cross sections are investigated under FM→AFM phase transitions at low temperatures. The alloys are smelted in an induction furnace in a purified argon atmosphere from electrolytically refined Ni, Mn, and sponge iron, then diffusion-annealed for 48 h at 1,200K with subsequent water quenching. The temperature dependence of the real and imaginary components of the dynamic magnetic

susceptibility (DMV) and the nonlinear magnetic susceptibility of FeNiMn alloys, the temperature dependence of the dynamic critical index ν of the FeNiMn alloys, the static and thermal remanent magnetization of the FeNiMn alloys as a function of temperature, and magnetic phase diagrams of FCC alloys are plotted. The studies demonstrate that the spin glass-type frozen state forms within a broad temperature range in concentrated FCC FeNiMn alloys under an FM \rightarrow AFM concentrational phase transition where the interaction between the ferro- and antiferromagnetic critical correlations is significant. Yet in the alloys in which this interaction may be ignored, the PM \rightarrow SS temperature transition is usually a cooperative phase transition at a nonzero critical temperature. The authors are grateful to A.Z. Menshikov and B.N. Mokhov for providing samples. Figures 4; references 19: 11 Russian, 8 Western.

Structure of Surface Layers Forming Under Water-Cooled Nickel-Steel and Cobalt-Steel Pair Friction

927D0191I Kiev METALLOFIZIKA in Russian
Vol 14 No 1, Jan 92 pp 94-103

[Article by O.N. Razumov, Yu.F. Shavadskiy, Physics of Metals Institute at the Ukrainian Academy of Sciences, Kiev; UDC 539.621:539.211]

[Abstract] The structure of the surface layers forming during friction in Ni-steel and Co-steel pairs under cooling with water is examined from the viewpoint of both the characteristics of the physical and chemical processes occurring in real pairs and the properties of the alloys produced as a result of this interaction. To this end, the friction products produced in a 2070 SMT-1 friction machine by the shaft-block mechanism at a slip rate within a 2-4 m/s rate under a 100 N load are studied. The shaft is made as a steel disc while the block is made from nickel or cobalt. The diffraction patterns of the friction products are produced in an HZG-4A diffractometer. Moessbauer spectra and hyperfine field distribution curves of the friction products obtained at various slip rates and the X-ray patterns of the friction products and their decomposition products at various slip rates are plotted. The relative fraction of the Moessbauer spectra components and the phase composition of the friction product components are summarized. Comprehensive analyses of the friction products show that alloys consisting of the friction pair constituents and the cooling medium are formed while the resulting alloys contain phases on the basis of solid solutions of the shaft and block materials as well as their oxides and hydroxides. A small change in the slip rate may lead to a significant change in the phase composition. The study also reveals the presence of an amorphous phase whose percentage fraction depends on the slip rate and peaks at 3 m/s. Figures 4; tables 3; references 10: 5 Russian, 5 Western.

Effect of Annealing on Local Structure of $Fe_{85-x}Co_xB_{15}$ Amorphous Alloys After γ -Irradiation

927D0191J Kiev METALLOFIZIKA in Russian
Vol 14 No 1, Jan 92 pp 104-110

[Article by V.V. Polotnyuk, A.M. Shalayev, V.M. Shkala, V.V. Kotov, Yu.F. Yurchenko (deceased), T.V. Yefimova, G. Vlasak, Physics of Metals Institute at the Ukrainian Academy of Sciences, Kiev; UDC 539.213:620.18]

[Abstract] The effect of γ -irradiation on the solidification temperature of $Fe_{85-x}Co_xB_{15}$ alloys, where $x = 12, 15, 17, 21$, or 25 , is investigated by thermomagnetic analysis of all alloys before and after the exposure. To this end, nuclear magnetic resonance spectra (YaMR) of the alloy with $x = 25$ are examined in the initial amorphous and irradiated states after annealing at a 380 and 700°C temperature for 15 min. Additional data on the solidification processes are also obtained by dilatometric analyses of an alloy with $x = 15$. The 10 mm wide and 30 μ m wide band samples for the study are prepared by quenching a flat jet on a spinning drum; the resulting samples are X-ray-amorphous. The dependence of the saturation magnetization on the heating and cooling temperatures before and after irradiation with γ -quanta, the nuclear magnetic resonance spectra before and after annealing and before and after irradiation, and the behavior of the linear expansion coefficient are plotted. The findings indicate that γ -irradiation leads to $FeCo \rightarrow Fe_3Co$ chemical transformation and $Z = 12 \rightarrow Z = 8$ topological transformation in the alloy and a change in the short-range order (BP) in the clusters which serve as the crystalline phase nuclei according to the polycluster model. The solidification onset temperature increases and the solidification interval expands due to a decrease in the cluster size. The solidification process occurs in two stages due to the presence of two types of short-range order clusters: $FeCo$ and Fe_3Co . The latter are still found after the amorphous alloy crystallization. Figures 3; tables 1; references 9: 8 Russian, 1 Western.

Structure Behavior of Rapidly Quenched Metal-Metalloid Alloys Under Exposure to Certain External Factors

927D0191K Kiev METALLOFIZIKA in Russian
Vol 14 No 1, Jan 92 pp 111

[Article by G.M. Zelinskaya, L.Ye. Mikhaylova, A.P. Brovko, A.V. Romanova, Physics of Metals Institute at the Ukrainian Academy of Sciences, Kiev; UDC 539.26:539.213:669.15]

[Abstract] The shortcomings of available data on the structural changes in metal-nonmetal alloys under the effect of external factors which are based on measurements of certain structurally sensitive properties are discussed, and the need to refine them, especially for the X-ray-amorphous structural state, is stressed. Consequently, the changes occurring in the structure of rapidly

quenched initially X-ray-amorphous alloys are studied by the X-ray diffraction analysis method, and attention is focused on establishing whether the character and origin of structural transformations under the effect of external factors, e.g., low-temperature annealing at 100°C for 200 h, irradiation with 1.2 MeV γ -quanta (with a total dose of 10^{-9} R), a 4 kbar all-around pressure, and melt overheating prior to solidification, in a number of alloys have common features. The structural factors and the functions of radial distribution of $4\pi r^2 p(r)$ atoms (FRRA) of rapidly quenched alloys before and after exposure are plotted. An analysis of diffraction patterns in MoK_{α} radiation and the results of transmission electron microscopy (PEM) studies show that real rapidly quenched alloys may contain a small quantity of small crystals which is consistent with theoretical predictions. For certain initial states, the effect of pressure and γ -irradiation may facilitate the crystalline phase breakdown while irradiation additionally affects the amorphous matrix state; the presence of the small crystals, however, does not significantly change the general diffraction pattern but merely increases the height of the first diffraction maximum. Irradiation and pressure tend to homogenize the alloy structure while low-temperature annealing, on the other hand, enhances the structural inhomogeneities and accelerates the onset of crystallization. The authors are grateful to D.Yu. Paderno for providing samples and N.D. Gadzyr for helping with electron microscopy. Figures 1; tables 1; references 16: 15 Russian, 1 Western.

Structural Factors Which Determine Reactor Graphite's Young Modulus Behavior After Irradiation and Annealing

927D0192A Moscow FIZIKA I KHIMIYA OBRABOTKI MATERIALOV in Russian No 3, May-Jun 92 pp 5-11

[Article by I.Ya. Levintovich, A.S. Kotosonov, Yu.S. Virgilyev, Moscow; UDC 661.66-532.21]

[Abstract] The effect of neutron irradiation at a relatively high fluence and low temperature and subsequent annealing on the Young modulus behavior of carbon materials in general and reactor graphite in particular is discussed, and the tenacity of materials with the graphite and turbostrate structure is determined. The effect of irradiation and subsequent annealing on the Young modulus and structural characteristics of the GR reactor graphite is studied and for comparison, the effect of annealing on irradiated graphite (OG) is compared to the similar effect of heat treatment on carbonized materials (KM), e.g., the GRP2 which has a higher density due to additional impregnation with tar. The dynamic Young modulus is examined by the speed of ultrasound propagation, the volumetric density is determined by measuring and weighing, the diamagnetic susceptibility is

measured by Faraday's method, and the electric conductivity and transverse magnetoresistance in a 1.7 T field are measured by the four-probe method. The study demonstrates that neutron irradiation at a 10^{20} - 10^{22} n/cm² flux at a 140-160°C temperature and subsequent annealing lead to a significant change in the reactor graphite tenacity. The macrostructure contribution to the decrease in the Young modulus reaches 40 percent while a considerable decrease in tenacity with a simultaneous increase in bulk density during the annealing is due to the opening of cracks and peeling as a result of a decrease in the layer spacing. The contribution of the void-free material volume makes the main contribution to the Young modulus variation in irradiated graphite during annealing. Figures 4; references 19: 9 Russian, 10 Western.

Assessing Optical Properties of Glass Materials Modified in Plasma Discharge by Infrared Spectroscopy

927D0192K Moscow FIZIKA I KHIMIYA OBRABOTKI MATERIALOV in Russian No 3, May-Jun 92 pp 65-68

[Article by M.K. Rodionov, N.P. Yevtushenko, V.I. Lobanov, V.I. Kuptsov, Yu.A. Shevlyakov, V.A. Terletskiy, Kiev; UDC 539.194:546.284:539.23]

[Abstract] The applications of structural composite materials on the basis of various types of glass fibers and the possibility of making them by varying the necessary thermal, mechanical, electrical, chemical, and optical properties are emphasized, and the optical properties and characteristic structural features of the T-10 and TS8/3K glass cloth modified by magnetron aluminum and graphite spraying are investigated. To this end, TS8/3K glass cloth made from quartz glass containing 99 percent silica and T-10 glass cloth made from silica, kaolin, limestone, and metal and nonmetal oxides are used as the original materials. The radiative heat transfer properties of the original and modified materials is evaluated on the basis of experimental reflection spectra in the middle infrared band in the Kirchhoff law approximation for the equality of emissivity and absorptance for transmitting bodies. The origin of the glass fiber is examined by the infrared spectra of samples pelletized with potassium bromide using a Specord 75 IK spectrometer. The glass fibers have a quasicrystalline origin and contain SiO_4 , AlO_4 , and AlO_6 structural groups. An analysis of the radiative heat transfer ability of the glass cloth surface with a 0.965 emissivity shows that the materials modified with aluminum and graphite by magnetron spraying are diffuse reflectors and may therefore be used for temperature stabilization of solar energy converters. Figures 2; references 11: 10 Russian, 1 Western.

'Third-Body' Formation and a Positive Mechanical Property Gradient Resulting From the Chemomechanical Application of a Brass Coating

927D0136A Minsk TRENIE I IZNOS in Russian
Vol 13 No 1, Jan 92 pp 67-70

[Article by G. Poltser, A. Firkovskiy, H.-J. Reinhold, V. Muller, J. Lange, V. Teppel, V. Retmayer, and L. Langkopf, Higher Technical Institute, Zwickau, Germany; UDC 621.891]

[Abstract] Three suppositions of adaptive system theory as it applies to friction pairs were utilized to develop a chemomechanical method of applying brass coatings. The coating process is primarily based on the phenomenon of third-body formation, in this case the formation on the friction surfaces of an extremely fine layer of brass with mechanical properties that are completely different than the basis metal. The coating is applied by having a brass reamer rotate against the surface of a steel or iron part while bathed in FPT-1 fluid, which contains copper. This process increases by as much as 30 percent the shear strength of the surface of the material to a depth of 80 μm and creates a stable coating with both a layer of brass with a completely new structure and an intermediate layer 2-4 μm thick between the brass coating and the basis metal. The tribomechanical processes at work here also create a top layer of copper. In addition to the creation of a bond between the coating and the treated surface, the microgeometry of the friction surfaces is optimized, and lubricant adhesiveness is improved. The application of this process, which only requires a few minutes and can be automated, has numerous advantages, including low material and energy consumption, a noticeable decrease in friction and part wear, and no harmful environmental effects. The new process can be effectively used on cylindrically shaped iron and steel parts to reduce friction, wear, tribocorrosion, fatigue failure, and seizing. Figures 1; references 10: 5 Russian, 5 Western.

Model of Coating Interaction That Accounts for Deformability, Wear, and Heat Liberation

927D0136C Minsk TRENIE I IZNOS in Russian
Vol 13 No 1, Jan 92 pp 154-160

[Article by V. M. Aleksandrov and G. K. Annakulova, Institute of Problems of Mechanics, USSR Academy of Sciences, Moscow; UDC 539.375]

[Abstract] A model of friction interaction between two surfaces with elastic coatings was presented. The model accounts for deformability, wear, and heat liberation. In this model, two flexible coatings with different initial thicknesses and different mechanical and thermophysical properties are applied to non-deforming substrates. The two bodies are slowly compressed by varying levels of force and, at a specific moment, one body begins to slide at a constant rate of speed against the other in the direction of the z axis. The forces of friction that arise at the boundary between the two layers induce wear in the

coatings and create time-specific work, much of which turns into heat, primarily within the "third-body" layer, which nearly coincides with the x axis. Heat sources in the form of tiny defects that cause friction are distributed throughout this layer, which thus has variable thermal conductivity throughout its thickness. Thus, the first step is to determine the thermal conductivity of this layer. The next step entails solving the quasi-stationary problem of thermal conductivity for two layers, accounting for the linear relationship between the coefficient of friction and the contact surface temperatures. While solving this problem, the conditions that make quasi-stationary thermal conductivity feasible and that give rise to thermal shock are determined. In step three, change in coating thickness as a result of friction-induced wear is calculated. It is then a simple matter to determine how long it will take for one of the layers to become completely worn. Two ways to solve this problem are discussed. Finally, wear caused by friction-induced fusion of the surfaces is examined. Figures 2; references 8: Russian.

Crystallization and Magnetic Properties of Co-P-Re Amorphous Electrolytically Precipitated Films

927D0191H Kiev METALLOFIZIKA in Russian
Vol 14 No 1, Jan 92 pp 82-87

[Article by M.U. Sheleg, L.V. Nemtsevich, T.A. Tochitskiy, N.N. Kozich, Solid State and Semiconductor Physics Institute at the Belarussian Academy of Sciences, Minsk; UDC 539.213.27]

[Abstract] The importance of amorphous films of iron-group metal alloys with phosphorus for practical applications due to their unique combination of magnetic, mechanical, and resistive characteristics and the variability of the physical properties of these films under the effect of irradiation, heating, and pressure prompted an investigation of the effect of rhenium additions on the microstructure and magnetic properties of amorphous and crystallized Co-P-Re alloy films. To this end, 0.04-1.0 μm films containing 9-22 percent P and 0.3-1.7 percent Re produced by electrolytic precipitation from sulfate-perrhenate electrolytes on a polished foil substrate are used; structural studies are carried out under an EVM-100LM transmission electron microscope and DRON-3M X-ray diffractometer in CoK_{α} radiation. The coercive force, saturation field, and hysteresis loop squareness ratio are measured in an oscilloscope instrument, and the effective magnetic anisotropy constant is measured in a rotary anisotropy meter by Chikazumi's method. The chemical composition is determined by a photocalorimetry analysis while the HV hardness is measured in 10 μm samples in an mph-100 gauge. The solidification onset temperature is determined by X-ray and electron diffraction analyses. The dependence of the coercive force and adjusted perpendicular magnetic anisotropy constant (PMA) on the annealing temperature for films with various Re concentrations and the X-ray patterns of films with various Re concentrations

before and after annealing are plotted. The findings show that an addition of Re to an electrolytically precipitated alloy noticeably affects the properties of amorphous and crystallized films in that it increases the HV hardness and solidification onset temperature, retards the crystallization process, and changes the phase composition, leading to the development of rhenium phosphide. Figures 3; references 18: 15 Russian, 3 Western.

Plasma Spraying of ZrO₂-Based Sealing Coats

927D0192J Moscow FIZIKA I KHIMIYA OBRABOTKI MATERIALOV in Russian No 3, May-Jun 92 pp 58-64

[Article by S.T. Televnyy, V.S. Yesenbekov, N.M. Tverdyyin, I.P. Zakharova, Moscow; UDC 621.793.72.011:533.9]

[Abstract] The effect of the ratio of the clearance at the turbine blade end to the blade length on the turbine efficiency and performance indicators and the shortcomings of existing methods of making turbine seals are discussed, and the plasma spraying technology as well as the structure and properties of zirconium dioxide coats are investigated. These alternative ceramic sealing coat systems produced by changing step-by-step the plasma-sprayed coat composition make it possible to ensure a high operating temperature and improve the chemical resistance of the turbine. Nonstabilized zirconium dioxide powders and powders of ZrO₂ partially stabilized with 5, 7.5, and 10.4 percent Y₂O₃ are used as the source materials; the power particles are irregular in shape, porous, and have microcracks on the surface. The procedure for depositing the coat is outlined, the particle size distribution is plotted, and the structure, friction layer composition, density, porosity, and gas abrasive resistance of the plasma-sprayed ceramic coats are summarized; the coats are deposited on high-temperature nickel alloys VZh101, ZhS6U, and VZhL12u. An X-ray phase study of the coats is carried out in CoK_α radiation using a DRON-3 diffractometer. An analysis of the methods of decreasing thermal stress in plasma-sprayed coats shows the importance of increasing the number of pores or microcracks for improving the thermal resistance of the coats and reveals that powders with 20-60 μm particles are the most suitable since they help to produce the necessary coat porosity. A decrease in the thermal erosion stability of the coats with an increase in the stabilizing yttrium oxide is noted; it is shown that at a 7 percent Y₂O₃ concentration, the microcracks forming in the surface layer serve as a barrier for the development and spread of macrocracks. Figures 4; tables 1; references 7: 1 Russian, 6 Western.

Corrosion-Resistant Aluminide-Class Diffusion Coats on High-Temperature Alloys

927D0192L Moscow FIZIKA I KHIMIYA OBRABOTKI MATERIALOV in Russian No 3, May-Jun 92 pp 80-84

[Article by A.A. Kopylov, O.V. Dvoretskiy, Yu.G. Vekslar, V.P. Lesnikov, V.P. Kuznetsov, S.F. Rybkin, Yekaterinburg; UDC 669.24:669.861]

[Abstract] Technical obstacles to increasing the corrosion resistance of aluminide-class coats by comprehensively alloying them with such elements as Co, Cr, Si, and rare earth metals (RZM) which lead to powder caking and even fusing are discussed, and it is noted that the contactless gas circulation method (GTsM), which makes it possible to separate not only the alloying mixture from the parts in the reaction volume but also the individual alloying composition components, is free of these shortcomings. Consequently, the possibility of producing multicomponent coats on a nickel alloy by the gas circulation method is investigated, and the properties of the multicomponent coats are evaluated. The ZhS6U age-hardenable corrosion resistant alloy is used as the base; the alloying process is carried out for 3.5-4.5 hours at a 1,000 +/- 25°C temperature, and vacuum annealing is conducted for two hours at 1,050°C. Crucible corrosion tests are performed in a salt coating. The metallographic, X-ray structural, and X-ray spectral microanalysis methods are used to examine the coat properties. The dependence of the Al activity on its concentration in the Co-Al system and the element distribution in the NiCoCrAl coat are plotted, and the results of the elemental analysis of the alloyed coats are summarized. Preliminary data show the need for additional powder processing by vibration treatment in a pseudofluidized bed. A combination of the two procedures with a correct catalyst makes it possible to improve considerably the corrosion resistance properties of high-temperature alloys with aluminide diffusion coats, extend their service life, and expand their operating temperature range. Figures 4; tables 1; references 6.

Production of Powders Reinforced With Silicon Carbide Discrete Particles and Filamentary Crystals

927D0192O Moscow FIZIKA I KHIMIYA OBRABOTKI MATERIALOV in Russian No 3, May-Jun 92 pp 126-130

[Article by I.Ye. Kalashnikov, V.N. Meshcheryakov, T.A. Chernyshova, T.V. Korzh; Moscow; UDC 669.018]

[Abstract] The outlook for composites on the basis of light metal alloys reinforced with discrete ceramic fillers such as particles, short fibers, and filamentary crystals and the shortcomings of the solid phase combining methods are discussed, and the prospect for making composites in two stages is outlined. The method of making composite powders by centrifugal spraying of a consumable composite electrode that is fabricated by compacting a mixture of metallic powder and discrete filler, i.e., silicon carbide, is studied, and the shape of the resulting powders is examined as a function of the spraying parameters and crystallizer type as well as the type of reinforcing filler distribution. The proposed technology makes it possible to attain a good bond between the components due to the wetting of the reinforcing filler by the matrix metal and produce composite mixtures with a uniform or functional reinforcing filler distribution. SiC particles with a 5 μm size and SiC filamentary crystals (NK) with a mean 0.14 μm

diameter and $\geq 50d$ length are used as the reinforcing filler, the PTEK-1 Ti powder and AD-1 Al powder with a $< 100 \mu\text{m}$ size are used as the matrix metal. The composite powders with a 200-600 μm matrix size are produced and their properties are investigated; the study confirms the possibility, in principle, of producing a composite metal powder reinforced with a discrete ceramic filler by the

method of centrifugal consumable electrode spraying whereby the reinforcing silicon carbide filler maintains its original phase composition. The method makes it possible to produce powders with matrices from chemically active and even refractory metals, which is impossible to do by other methods. Figures 4; references 4: 2 Russian, 2 Western.

Matrix Synthesis—A New Method of Polymeric Low-Friction Composite Materials

927D0136D Minsk TRENIYE I IZNOS in Russian
Vol 13 No 1, Jan 92 pp 195-200

[Article by I. A. Gribov, G. I. Gureyev, A. I. Kuznetsov, A. P. Krasnov, V. A. Vasnev, S. V. Vinogradova, V. N. Ignatov, Ye. M. Belavtseva, and A. I. Lapshin, Institute of Elementary Organic Compounds of the USSR Academy of Sciences, Moscow; UDC 541(127+64):542.954]

[Abstract] The friction properties of a new polymer composite material made by matrix synthesis were studied. The material is based on linear dichlorodian polyterephthalate synthesized by acceptor catalyzed polyesterification in the presence of C-1 graphite filler. Filler concentration was 30-60 wt. percent. Material specimens were applied in the form of coatings approximately 30 μm thick to metal bushings 22 (diameter) x 12 mm. The properties of these coatings were compared

with those of conventionally made polymer composite coatings. Friction tests were performed on a tester that accommodates face-to-face contact with an approximately 0.1 MPa load and a sliding contact speed of about 0.3 m/s. Photomicrographs were taken on an Hitachi S-2500 scanning electron microscope. Free surface energy was measured from angle of contact measurements. The results of the tests showed that coatings made from the new composite had a much lower coefficient of friction (0.2 vs 0.8) than the other test coatings and had a 66 percent reduction in wear-induced loss of mass. The reduction in wear-induced loss of mass was especially noticeable during the running-in period. Also, the piece of counteracting steel used in the test also suffered less wear, as it acquired a film of the low-friction coating during the testing. The improved friction properties of the new coating material were attributed to enhanced structural characteristics such as higher molecular mass and characteristic viscosity resulting from the particular features of polymer structure formation on the surface of the filler. Figures 4, tables 2; references 6: Russian.

Improving the Corrosion-Resistance of Chromized Parts Made From Iron Powder

927D0177E Kiev POROSHKOVAYA
METALLURGIYA in Russian No 4, Apr 92 pp 28-31

[Article by I. S. Litmanovich and Ya. M. Zolotovitskiy, Technopribor Special Design Bureau, Gomel; UDC 621.793.6]

[Abstract] The possibility of increasing the corrosion resistance of chromized parts made from iron powder was examined. Specimens in the shape of 5 x 15 x 30-mm rectangular parallelepipeds were pressed from PZhR V3.200.28 iron powder and sintered at 1150°C for two hours in an Rx-gas atmosphere. Corrosion-resistance was imparted to the specimens in one of six ways: conventional chromizing; conventional chromizing and impregnation with PK-80, an anaerobic organic compound capable of polymerizing; conventional chromizing, impregnation with PK-80 and passivation in a solution of potassium bichromate; chromizing with pre-carburization of the iron; pre-carburization, chromizing, and impregnation with PK-80; and pre-cementation, chromizing, impregnation with PK-80, and chemical passivation. Comparative corrosion resistance tests were then performed on 5-specimen batches exposed to a total of 10 cycles, each of which consisted of two parts. First,

the specimens were exposed for eight hours to a temperature of 35 + 2°C and a humidity of 95 + 3 percent, after which the specimens were exposed to a humidity of 100 percent and a gradual decrease in temperature from 35° to 20°C over a period of 16 hours. The results of the tests showed that specimens that had been chromized after pre-cementation, impregnated with the PK-80, and then passivated in the potassium bichromate solution exhibited no signs of corrosion damage. This process makes parts made from iron powder much more versatile and capable of being substituted for parts made of much more expensive high-alloy chromium and nickel-chromium steels. Tables 1; references 3: Russian.

Protective Coatings for Niobium, Tantalum, Molybdenum, and Tungsten To Increase Resistance to High-Temperature Oxidation

927D0177G Kiev POROSHKOVAYA
METALLURGIYA in Russian No 4, Apr 92 pp 37-41

[Article by Yu. V. Dzyadykivich, Ternopol Pedagogical Institute; UDC 621.793]

[Abstract] Various methods of applying high-temperature oxidation-resistant coatings to niobium, tantalum, molybdenum, tungsten, and their alloys are surveyed. Figures 1; references 26: 18 Russian, 8 Western.

Implantation of Nitrogen Together With Carbon or Oxygen in Molybdenum

927D0182H Moscow POVERKHНОСТ: FIZИKA, KHIMИYA, MEKHANИKA in Russian No 10, Oct 92
pp 138-143

[Article by Kh. R. Kazdayev, Ye. M. Bayadilov, M. T. Akchulakov, D. K. Daukeyev, I. V. Khromushin, and Zh. R. Zhotabayev, Institute of Nuclear Physics of the Kazakh Academy of Sciences, Alma-Ata; UDC 639.2:669.285]

[Abstract] The behavior of nitrogen implanted in molybdenum was studied to determine how it is affected by supplemental alloying of the Mo with carbon or oxygen atoms. The specimens used in the study were Mo single crystals, 99.96 percent pure, cut along the plane (110) to make 8 x 1.5-sq mm rectangles 1 mm thick. The specimens were implanted with ^{15}N isotopes with 45 keV of energy at a dose rate of $5(10^{17}) \text{ cm}^{-2}$, and then implanted with ^{13}C (40 keV; $5(10^{16}) \text{ cm}^{-2}$) or ^{18}O (50 keV; same dose rate as for C). The specimens were then isochronally annealed in a vacuum for one hour at 100° intervals from 200 to 1200° [as published]. X-ray diffraction analysis, performed with the aid of a glancing X-ray beam, was used to examine the near-surface layer structure. Thermal desorption spectroscopy of the N was done using an automated high-vacuum apparatus in a differential mode while heating the specimens at a rate of 1%/s. The introduction of nitrogen into monocrystalline Mo leads to the formation of corresponding nitrides, the dissociation of which during annealing is accompanied by the diffusion of the N into the matrix and its subsequent release from the specimens. Additional alloying with C or O not only lowers the temperature of N

dissociation, but also greatly affects the rate of N desorption within various temperature ranges. It is thought that the phenomena observed are caused by the formation of Mo carbo- and oxy-nitrides, by the carbidization of the specimen surfaces, and by the change in the diffusivity of the nitrogen in the molybdenum in the presence of the alloying mixtures used. Figures 4, tables 1; references 11: 8 Western, 3 Russian.

Low-Temperature Diffusion of Platinum in Thin Copper Films

927D0182I Moscow POVERKHНОСТ: FIZИKA, KHIMИYA, MEKHANИKA in Russian No 10, Oct 92
pp 152-154

[Article by A. N. Aleshin, V. K. Yegorov, and P. V. Kurkin, Moscow Institute of Steel and Alloys; UDC 539.216.2:539.219.3]

[Abstract] The thickness of thin platinum and copper films applied to a GaAs substrate was estimated from changes in electrical resistivity, and these measurements were then refined with the aid of Rutherford backscattering. The films were produced by sequential magnetron spraying. To measure the coefficient of Pt diffusion into the Cu at room temperature, film specimens were kept for 40 months, after which Rutherford backscattering spectra of the He+ ions were recorded. Measurement accuracy was enhanced by a system of parallel independent two-channel registration, which made it possible to detect scattered ions at 160- and 145° angles. The results showed that, at room temperature, Pt diffusion into Cu occurs, for practical purposes, only along the grain boundaries, in the "C" mode, and corresponds to the value for the coefficient of bulk diffusion at this temperature [$(3.0+0.3) \times 10^{-18} \text{ sq cm/s}$]. Figures 1; references 8: 7 Western, 1 Russian.

Using Cement Plant Electrostatic Precipitator Dust in Glassmaking

*927D0180A Moscow STEKLO I KERAMIKA
in Russian No 3, Mar 92 pp 3-5*

[Article by N. I. Minko and K. I. Yermolenko, Belgorod Technological Institute of Building Materials; UDC 666.1:691.54.0048]

[Abstract] The feasibility of using dust collected from the upper fields of the electrostatic precipitators in the Belgorod cement plant to make packaging glass was examined. The chemical composition of the dust was (percent): 8.75 silicon dioxide, 36.14 calcium oxide, 0.3 magnesium oxide, 2.69 aluminum oxide, 4.0 sodium monoxide, 23.0 potassium oxide, 1.75 ferric oxide, and 2.37 sulfur trioxide. The active lime content of the dust was 8.35 percent. In addition to the dust, the charge also consisted of Lebedin sand, belgorod chalk, dolomite, soda, and alumina. A small amount of carbon was added to reduce the sulfates. The raw materials were sifted through a No. 9 screen, dried at 300°C until the moisture content was 0.5 percent, weighed, and mixed in a laboratory ball mill or blade mixer for 15 minutes. The glasses were made at a temperature of 1450°C in a laboratory electric furnace in 100-ml fused alumina crucibles and in a gas-fired crucible furnace in 2-l fireclay crucibles in a slightly oxidic atmosphere until the molten glass was completely clear. The glass was poured into 50 x 50 x 10-mm molds. Standard techniques were used to measure its properties. The data showed that glass made with the dust met packaging glass specifications. Higher dust concentrations lower the amount of soda required, but too high a concentration can adversely affect viscosity and crystallization. The ideal ash concentration is 6.64 percent; this reduces soda consumption from 26.4 to 24.03 parts per 100 kg of glass mass and completely eliminates the need for chalk without having a deleterious effect on processing or molding characteristics. The active lime in the dust accelerates the vitrification process. It takes somewhat longer for the molten glass to clarify because of the finely dispersed nature of the dust, but this effect can be largely offset by lightly compacting the charge into briquettes. Figures 1, tables 2; references 2: Russian.

Selecting Process Duration and Temperature When Molding Glassware From Sheet Glass

*927D0180B Moscow STEKLO I KERAMIKA
in Russian No 3, Mar 92 pp 5-6*

[Article by A. G. Shabanov, N. V. Lalykin, A. I. Shutov, and V. P. Markov, Tekhstroysteklo Scientific Production Association and the Belgorod Technological Institute of Building Materials; UDC 666.151.035.2]

[Abstract] The process of molding glassware from sheet glass was modified to take advantage of the higher relaxation stresses that accompany a longer molding time while compensating for the deleterious elastic and chilling effects that also accompany longer molding

times. Essentially, the modified process entails setting the duration of the molding process so that maximum relaxation stress values are obtained, compensating for the elastic consequences by increasing the curvature of the shaped ware, and combatting the chill factor by heating the glass to a higher-than-usual temperature prior to molding. The mathematical equations and nomogram utilized for this purpose were adduced and applied to a concrete production problem. Figures 2; references 2: Russian.

Producing Photochromic Glass From a Synthetic Charge

*927D0180C Moscow STEKLO I KERAMIKA
in Russian No 3, Mar 92 pp 7-9*

[Article by A. B. Atkarskaya, O. I. Mironenko, F. A. Tkachenko, V. A. Tsekhomskiy, V. S. Shashkin, and L. P. Yurchuk, State Optical Institute imeni S. I. Vavilova and the Izyumsk Instruments Plant; UDC 666.247]

[Abstract] The use of synthetic charges to make high-quality photochromic glass was investigated. The conventional charge was made by dry mixing pure nitrates, carbonates, boric acid, oxides, and silica powder in the normal manner. The synthetic burdens were made by mixing solutions containing silicon sol and ions of the other components. The resulting colloid was gelled for one to 30 minutes depending on pH, temperature, and component concentrations and then heat-treated at 150-200°C. The glasses were made in a laboratory electric furnace with Silit heating elements in crucibles made of silica glass, stekrite, or corundize with 100 to 150-ml capacities. The batches were charged at 1200 or 1350°C. The molten glass was clarified for three hours at 1360-1480°C, poured into 30 x 70 x 15-mm metal molds and annealed in a laboratory muffle furnace at 460°C. Inclusion frequency and size was studied on an MIN-8 microscope, a chemical analysis was performed to determine aluminum oxide content, and photochromic properties were assessed on an IFS-2 spectrophotometer. Parallel glass batches were used to ensure test reproducibility. The results showed that the use of synthetic charges improves the quality of photochromic glass by totally eliminating incomplete melting, even at relatively low temperatures (e.g. 1360°C). Thus, the glassmaking temperature can be decreased, inclusions eliminated, and refractory corrosion reduced. Since Na₂O-B₂O₃-SiO₂ is the most corrosive and difficult component to melt down, charge formulation can be simplified by chemically synthesizing this particular component and adding the remaining as if formulating the charge in the conventional manner. Figures 2, tables 4; references 4: Russian.

Outlook for Powder-Process Glass Ceramics

*927D0180D Moscow STEKLO I KERAMIKA
in Russian No 3, Mar 92 pp 12-14*

[Article by V. I. Solovyev, Ye. S. Akhlestkin, E. P. Sysoyev, and A. A. Tryapkin, Vladimir Polytechnic Institute]

[Abstract] The two major technologies for producing glass ceramics were compared. Although it is more expensive, labor- and energy-intensive, and complex, powder-process glass ceramics technology has numerous advantages over glass ceramics processes based on traditional glassmaking methods. These advantages include greater product diversity and versatility, superior physical, chemical, mechanical, and service properties, the relative ease with which these products can be "customized" to have specific blends of high-performance properties and characteristics, and lower material utilization and costs. Organizations such as the State Glass Institute, the Moscow Institute of Electronics Technology, Vladimir Polytechnic Institute, the Moscow Institute of Chemical Technology imeni D. I. Mendeleyev, the Belorusian Institute of Technology imeni S. M. Kirov, Tomsk State University, and the Institute of Applied Materials Science are working to develop more and more applications for powder-process glass ceramics. Figures 2, tables 1; references 9: 8 Russian, 1 East European.

Optical Constants of Bismuth Containing Ga Glasses

927D0180E Moscow STEKLO I KERAMIKA
in Russian No 3, Mar 92 pp 15-16

[Article by A. I. Rabukhin and G. V. Belousov, Moscow Institute of Chemical Technology imeni D. I. Mendeleyev; UDC 666.112.9:546.681:546.87]

[Abstract] The optical properties of bismuth-gallium glasses synthesized within the CdO-Bi₂O₃-Ga₂O₃ and PbO-Bi₂O₃-Ga₂O₃ systems were studied. The glasses were made from c.p. CdO, Pb₃O₄, Bi₂O₃, and Ga₂O₃ reagents in fused-alumina crucibles in an electric furnace with Silit heating elements at 1050-1100°C. The melt was poured onto a cooled steel slab, and the glass baked at 350-400°C. Chemical composition was monitored by quantitative X-ray spectrometry on a Comebax [as published] microspectrometer. Variation in glass composition did not exceed 1 percent from batch to batch. Aluminum oxide concentration did not exceed 3 percent. Refraction was measured on a GS-5 goniometer at four mercury spectrum wave-length values; transmission spectra were recorded on a Specord M40 spectrophotometer. The data showed that an increase in the concentration of oxides containing highly polarized Pb₂₊ and Bi³⁺ cations leads to a substantial increase in refractivity and the average dispersion of the glasses studied, while an increase in Ga₂O₃ leads to a reduction in these values due to the replacement of the lead and bismuth oxides. Figures 2, tables 5; references 4: 2 Russian, 2 Western.

Fractal Properties of Interfaces in Zirconium Dioxide Powders Produced Using Plasma Chemistry Processes

927D0180F Moscow STEKLO I KERAMIKA
in Russian No 3, Mar 92 pp 20-21

[Article by Yu. A. Abzayev, N. V. Dedov, Yu. F. Ivanov, and A. V. Paul, Tomsk Construction Engineering Institute; UDC 669.017.620]

[Abstract] Electron diffraction microscopy of zirconium dioxide powders revealed that their grain structure is fractal in nature. Fractal dimensionality increases as grain size decreases; conversely, the larger the grain size, the closer the ratio of grain size to fractal dimensionality gets to unity. Comparative studies of calcium oxide showed that the conditions under which a material is made play a critical role in the formation of fractal structures. The fractal nature of zirconium dioxide indicates the presence of high elastic distortions in the structure of the material. For this reason, products compacted from this powder need to undergo relaxation annealing in order to avoid warping or failure. Figures 1; references 7: 3 Russian, 4 Western.

Phase Transformations When Firing Ceramic Tiles Made Primarily of Ore-Dressing Gangue

927D0180G Moscow STEKLO I KERAMIKA
in Russian No 3, Mar 92 pp 23-24

[Article by V. Z. Adrakhimov, Ust-Kamenogorsk Division of the Scientific Research Institute of Building Materials Design; UDC 666.646.66.046.514]

[Abstract] Radiographic, IR-spectroscopic, and microscopic methods were used to study the effect of light ash on phase transformations when firing ceramic tiles made of ore-dressing gangue. The tiles were made in a conventional manner of 60 percent zirconium-ilmenite gangue and 40 percent ash. Tile dimensions were 100 x 100 x 10 mm. The tiles were fired at 900-1200°C. The study showed that the addition of the ash intensified phase transformation processes in this ceramic and prevented formation of crystallobite, which adversely affects the physical and mechanical properties of the material. Figures 4; references 5: Russian.

Increasing the Stability of Enamel Slips for Composite Coatings

927D0180H Moscow STEKLO I KERAMIKA
in Russian No 3, Mar 92 pp 25-26

[Article by L. A. Kurakevich, I. V. Stefanyuk, L. G. Khodskiy, and A. A. Sirotinskiy, Institute of General and Organic Chemistry of the Belorusian Academy of Sciences; UDC 666.293.521.34]

[Abstract] Several different mineral and colloid-forming additives were studied to determine their effect on the sedimentation stability of composite coating slips. The enamels studied were based on the R₂O-RO-B₂O₃-SiO₂ system with cohesion-activating additives. The charges were made from glass sand, chalk, soda ash, aragatsk perlite, and sodium octaborate from the Bor Production Association. The mineral additives included finely ground glass sand, nepheline concentrate, marshalite, glass powder, and other materials. Although coating performance improved, slip stability decreased, so 0.3-0.5 percent magnesite, andesite powder, diatomite, basalt, and various lithium salts were added to improve

stability. A technique developed by Novocherkassk Polytechnic Institute was used to measure the sedimentation stability of the enamel slips. Precipitation kinetics as a function of aging time and type of additive were also studied. The basalt, LiCoO_2 , Li_2SiO_3 , and andesite helped to improve slip stability; the other additives either had adverse or insignificant effects. Of all the additives, basalt was the most effective. Optimal slip composition consisted of 100 parts (in mass units) of enamel frit plus six parts Chasov Yar clay, 20 parts finely ground glass sand, 0.4 parts crystal borax, 0.2 parts sodium nitrite, 0.3-0.5 parts basalt, and 50-55 parts water. The slip was tested on Steel 10 specimens. Firing temperature was 880-900°C. The coatings had high thermomechanical properties: heat resistance was 370-400°C, impact strength—3.1-4.9 J. The coatings performed well in tests simulating industrial conditions and is recommended for use on large pieces of equipment, including pipe, to enhance their thermomechanical characteristics. Figures 1, tables 1; references 2: Russian.

Relaxation Properties of Enamel Slips

927D0180I Moscow STEKLO I KERAMIKA in Russian No 3, Mar 92 pp 27

[Article by A. V. Nikitenko, Novocherkassk Polytechnic Institute; UDC 666.29.022.7]

[Abstract] The relaxation properties of enamel slips with chemical compositions corresponding to ESG-21, ESG-26, ESG-31, and ESP-117 enamels were studied on a Weiler-Rebinder relaxometer. Slip density was 1520 to 1710 kg/cu m. The sensing element was a corrugated plate 10 sq cm in area; an induction sensor was used to monitor its movement, which was recorded by a plotting device. The structure of the suspensions was first destroyed by agitating them in a mixer. The suspensions were then poured into the cell of the test instrument, and the plate immersed in them. The samples were left alone for five to 50 minutes or for 24 hours to allow them to recover their structure. They were then subjected to shear deformation by repeatedly loading the instrument's sensing element. The distance between the wafer and the cell wall was 0.01 m. The mechanical properties of the slips' structure were also measured from a number of elasticity and viscosity parameters. The data showed that, after a 24-hour structural recovery interval, the true relaxation period for protective enamels lasted for 1.5 s. For the primer enamels, the true relaxation time varied from 1.6 to 1.8 s when recovery time was increased from 50 minutes to 24 hours. The enamel slips recover their structure within 0.88 to 1.88 s after agitation is ceased. These data show that it is important to take structural recovery time into account when applying enamel coatings, especially when using mechanical enameling equipment to do so. Figures 1; references 2: Russian.

Factors Affecting the Formation of Solid Solutions in Strontium-Barium Glass Ceramics

927D0181A Moscow STEKLO I KERAMIKA in Russian No 2, Feb 92 pp 7-9

[Article by N. M. Bobkova and L. M. Silich, Belorusian Institute of Technology imeni S. M. Kirov; UDC 666.263.2]

[Abstract] In order to establish the factors affecting the formation of solid solutions in the strontium-barium system, five types of glass were synthesized. The glasses consisted of various ratios of SrO to BaO , including those made purely of either one or the other element, 10, 15, 20, and 25 percent Al_2O_3 , and 12.5 or 15 percent TiO_2 . The glasses crystallized between 950 to 1200°C. X-ray phase analysis of the glasses showed that three main factors affect the formation of solid solutions: processing temperature, aluminum oxide concentration, and the $\text{SrO} : \text{BaO}$ ratio. In all of the glasses of either pure strontium or barium composition, either the triclinic form of strontium anorthite formed, or monoclinic celsian did. As the quantity of aluminum oxide was increased, the temperature at which the high-temperature forms turn into the low-temperature forms decreases, especially in compositions with elevated concentrations of barium oxide. Between 950-1000°, the solid solutions form only in glasses containing at least 20 percent aluminum oxide, with the triclinic strontium anorthite predominating, even when there is a much higher concentration of BaO than SrO . As the temperature is increased, the solid solutions appear at lower concentrations of aluminum oxide—15 percent at 1100°C and 10 percent at 1200°C. Strontium anorthite still predominates unless the $\text{SrO} : \text{BaO}$ ratio favors the latter. Although the different types of glass seemingly form a continuum in terms of structure and properties, the characteristics of the glasses made with the oxides are superior to those made without them. Figures 3; references 2: Russian.

Absorption by Pigments in FK-14 Glass

927D0181B Moscow STEKLO I KERAMIKA in Russian No 2, Feb 92 pp 10-11

[Article by A. B. Atkarskaya, V. I. Borulko, V. A. Krivulya, S. Z. Khripunov, and Yu. V. Shevchenko, Scientific Research Institute of Automotive Glass; UDC 666.295]

[Abstract] The specific spectral and integrated absorptivities of bi- and tri-valent iron, bi-valent copper, nickel, and cobalt, and tri-valent chromium were determined and used to establish the effect of these elements on the absorption of light in the visible and near-IR spectral regions. The oxides or salts of these elements were added to laboratory-synthesized glass made from c.p. or h.p. materials. The glass was made in 200-ml silica glass crucibles in a furnace with Silit heating elements. The molten glass was poured into metal molds and annealed in a muffle furnace to make plane-parallel plates of

various thicknesses. The spectral coefficient of the transparent glass was measured on an SF-26 spectrophotometer within a wave-length interval of 360-1100 nm, and the integrated coefficient was measured on an FM-94M photometer. The concentration of bi-valent copper ranged from 82-99 percent, an amount that is 10-30 times more than the bi-valent copper concentration in silicate glasses. Evidently, the phosphate matrix of the FK-14 glass has a greater oxidizing effect on copper. Chrome, nickel, and cobalt ions have the greatest absorptivity within the visible spectral region. Bi-valent iron, nickel, and copper greatly increase the loss of light in the IR region of the spectrum. Figures 1, tables 1; references 1: Russian.

Densely Sintered and Porous Glass Ceramic Dielectrics

927D0181C Moscow STEKLO I KERAMIKA
in Russian No 2, Feb 92 pp 16-18

[Article by V. I. Solovyev, V. A. Leshina, I. A. Denisyuk, V. N. Petrova, F. M. Orlova, and S. V. Borisova, Vladimir Polytechnic Institute; UDC 666.263.2:537.226]

[Abstract] The dielectric properties of a number of different glass ceramics made using powder technology were studied. The materials were made from silica sand, lime, dolomite, alumina, and small concentrations of other pure materials. Semi-wet pressing was used to compact the powdered glass, which was treated with paraffin plasticizer, polyvinyl alcohol, and silicone binders. Five MPa of specific pressure was used to press the compacts for the porous specimens, and 100 MPa for the densely sintered specimens. The compacts were fired in reverberatory furnaces under the following conditions: increasing the temperature at 100-200°C/h, pre-sintering the specimens at 300-400°C for one to two hours to burn out the plasticizer, setting a final firing temperature of 850-1300°C depending on the type of material, and holding the specimens at that temperature for 0.5-two hours. Glass ceramic cements and coatings were applied conventionally and underwent accelerated heat treatment. It was found that permittivity in glass ceramics with the same chemical and phase compositions depends largely on relative density and overall porosity, which are functions of sintering conditions. The nature or size of the pores has virtually no influence. In contrast, the $\tan \delta$ (loss angle tangent) has a complex relationship to pore size and nature and increases as pore size and the proportion of closed pores increase. Depending on pore structure, porous materials can have a $\tan \delta$ equal to that of densely sintered materials. Dielectric characteristics are also affected by component heterogeneity. Sealing the surface of the materials has virtually no effect on dielectric properties. Thus, glass ceramic dielectric materials can be made extremely versatile by varying their chemical and phase compositions, density, and porosity. Tables 3; references 1: Russian.

Alumino-Silicate Ceramic With BaO-CaO-SiO₂ System Eutectic Additive

927D0181D Moscow STEKLO I KERAMIKA
in Russian No 2, Feb 92 pp 20-21

[Article by G. A. Afonina, V. G. Leonov, and L. A. Beresnevich, Moscow Institute of Chemical Technology imeni D. I. Mendeleyev; UDC 666.762.1]

[Abstract] The composition of an alumino-silicate ceramic with an additive consisting of BaO-CaO-SiO₂ eutectic was mathematically optimized, and the characteristics of a compacting powder made from this material were studied. The ceramic was made from GKIS alumina and C-070-1 silica sand ground to a specific surface of 6000-6500 sq cm/g. The eutectic was added in the form of a mixture pre-synthesized at 1000°C. Optimal composition was calculated from a third-order regression equation to yield: 73.5 percent alumina, 13.2 percent silica, and 13.3 percent additive. The same technology used to make VK 94-1 alumina ceramic compacting powder was used to prepare a compacting powder from the experimental ceramic. The properties of this powder are equal to those of the VK 94-1 powder. A temporary process binder made with clay, polyvinyl alcohol, and glycerine helped reduce abrasive wear to the compacting molds and increase the output of usable compacts. Semi-wet pressing at 150 MPa of specific pressure was used to make compacts that were fired in a lab furnace at 1350°C with a two-hour holding period at the final firing temperature. The fired specimens had the following characteristics: water absorption—0.0 percent; average density—3.18 g/cu cm; bending strength—220 MPa; coefficient of linear expansion within a temperature range of 20-200°C— 53.5×10^{-7} K⁻¹; dielectric loss angle tangent— 10.7×10^{-4} ; permittivity—7.8; volume resistivity at 100°C— 8.1×10^{11} Om-m. The results of the study show that the new material is suitable for use in making integrated circuits. Figures 1, tables 2; references 3: Russian.

Mechanism of Surface Layer Formation When Grinding and Sharpening Ceramics

927D0181E Moscow STEKLO I KERAMIKA
in Russian No 2, Feb 92 pp 21-24

[Article by V. S. Fadeev, Institute of Machine Science and Metallurgy of the Far Eastern Division of the USSR Academy of Sciences; UDC 620.187:666.762.11]

[Abstract] The processes of structural formation and plastic deformation were studied in conventionally synthesized α -alumina-based ceramics. The bearing surfaces of interchangeable multifaceted plates made of VO13 oxide and VOK71 oxide-carbide ceramics were ground and sharpened on a ZYE642Ye machine tool with a diamond abrasive disk (APV 350 x 6 x 30 ASV 80/63 B1 100 percent). Cutting speed was 18 m/s, lengthwise tool speed was five m/min., and vertical tool speed was 0.02-0.25 mm for a double stroke. During machining, the parts were bathed in a 3 percent solution of sodium

carbonate. Specimen structure and grain morphology were studied on transmission and scanning electron microscopes using carbon replicas and chromium-shadowed specimens. The subgranular structure of the friction surfaces and the interior were examined on thin foils made by cathode etching a rotating specimen. Phase composition of wear products and thin foils was analyzed by quantifying microdiffraction patterns. Other methods of analysis used were: semi-quantitative isotope analysis on an EMAL-2 laser mass spectrometer; radiography; X-ray crystallography on a Linke 860-500 attachment to an ISM-35-SF electron microscope; and quantitative phase analysis on a DRON-3M diffractometer. The data showed that diamond abrasion machining leads to the formation of deformation defects on the oxide ceramic and to an increase in dislocation density in the oxide-carbide ceramic, defects that initiate brittle failure in these materials. Abrasive sharpening causes the formation of a secondary structure that has a dual effect on wear, the friction coefficient, and specific seizing force. Figures 5; references 7: 6 Russian, 1 Western.

Robot Arm for Applying Powdered Enamels

*927D0181F Moscow STEKLO I KERAMIKA
in Russian No 2, Feb 92 pp 24-25*

[Article by N. D. Parshin, Novocherkassk Polytechnic Institute; UDC 666.293.002.5]

[Abstract] A robot arm designed to apply powdered enamel coatings to cast-iron plumbing fixtures was described (inventor specification 1576303). The upper part of the arm is mounted on a housing that contains an asynchronous electric motor and a powder clutch unit. The forearm is equipped with a bracket that holds the enamel sprayer, which consists of a screen, a screen vibrator, and a metal hose connected to the powder supply. The arm is programmed directly by the operator, who uses a detachable handle to guide the screen along the desired path over the object to be sprayed. The control system converts the analog information coming from the motion sensors into a 12-bit binary code and stores it in a digital memory that can remember 200 seconds or more of continuous motion. At the same time the motion is being programmed, the commands for starting the vibrator, powder dispenser, and so forth are also stored. A positioning device that holds the heated object being enameled is used in conjunction with the robot arm. It can cant the object at various angles to the horizontal and rotate it around a vertical axis, using a drive mechanism similar to the one used by the robot arm. The robot arm and the positioner share the same control system, and the positioner is also directly programmed by the operator. A special device was also developed to ensure consistent screen vibration and powder dispensation (I.S. 908949). The device consists of a phase sensor of screen load and a adjustable dispenser for feeding the powder through the hose onto the screen. Figures 1.

Polymer Coating for Ceramic Tile

*927D0181G Moscow STEKLO I KERAMIKA
in Russian No 2, Feb 92 pp 28*

[Article by D. N. Aneli, L. G. Shamaauri, M. A. Kinkladze, I. V. Karseladze, Georgian Scientific and Technical Institute of Power Engineering and Hydraulic Engineering Structures and Tblisi Technical University; UDC 666.7.05]

[Abstract] A polymer compound has been developed for coating the exposed surfaces of ceramic tile. The compound is made by thoroughly dissolving polyester resin in an equal amount of styrene, adding one part methyl ethyl ketone peroxide to initiate curing, thoroughly mixing, and adding one part cobalt naphthenate to hasten setting. A thin layer of the mixture is applied to the unglazed surface of a fired tile; a piece of window glass the same size as the tile is then placed on top of the treated surface of the tile. The tiles are allowed to sit for two hours at room temperature, after which they are placed in a drying oven where the coating is cured at 150°C for three hours and cooled to room temperature. The glass is easily removed to leave a smooth, even surface of sufficient hardness. Coating thickness varies from 300 to 400 µm. The polymer coating is highly water-, acid-, alkali- and corrosion-resistant, versatile, and can be produced in a wide variety of colors.

Study of Nb-Y₂O₃ System Powder Component Interaction

*927D0193A Moscow OGNEUPORY in Russian
No 6, Jun 92 pp 7-9*

[Article by A.Ye. Solovyeva, Sukhumi Engineering Physics Institute; UDC 546.882.001.5+546.641-31.001.5]

[Abstract] Component interaction in the Nb-Y₂O₃ powder system is investigated within a 25-2,000°C temperature range in a vacuum. To this end, phosphor-grade 99.990 percent pure yttrium oxide and MV-grade Nb with Ta, Ti, and other impurities are used; the samples for the study are prepared by traditional methods. The initial samples are examined by the high-temperature radiography method within a 25-1,800°C range in a vacuum in CuK_α radiation using an UVD-2000 adapter for the DRON-0.5 diffractometer at a 10°C/min sample heating rate. The lattice parameters are measured by plotting the (222), (400), and (622) yttrium oxide line profiles and (110) and (211) niobium line profiles accurately within 0.0001 nm. The sample are annealed before the study within a 600-2,000°C range in a vacuum. The sample microstructure is examined in reflected light using a MIM-8 microscope and by electron probe analysis in a MAR-1 unit. An analysis of the findings shows that niobium and yttrium oxide lattice cells interact within the 25-2,000°C range while niobium oxidation commences at 800°C; above 800°C, niobium oxides of different compositions form in the mixture. Yttrium oxide transformation to an ordered phase state occurs

within a 500-1,000°C while the lattice parameter of the disordered yttrium oxide phase varies within 1,100-1,300°C and remains constant within a 1,300-1,500°C range. Gaseous products form in the system at temperatures above 1,600°C while niobium oxides start dissolving in yttrium oxide at a 1,300°C temperature, forming a solid solution by substitution. The author is grateful to Yu.A. Malykhin for help. Figures 7; references 7.

Measurement of ZrO₂-Based Ceramics Static Modulus of Elasticity

927D0193B Moscow OGNEUPORY in Russian
No 6, Jun 92 pp 9-11

[Article by Ye.I. Akselrod, R.Ye. Volfson, Ukrainian State Scientific Research Institute of Refractories; UDC 666.762.5.017:539.32]

[Abstract] The importance of measuring the static modulus of elasticity of structural ceramics operating at constant static loads as a function of the temperature factors and production methods is emphasized, and the behavior of the static modulus of elasticity of structural ceramics on the basis of zirconium dioxide ceramics partially stabilized with magnesium and yttrium oxide is investigated. To this end, the static modulus of elasticity is measured within a temperature range from room temperature to 1,200°C in a unit designed at the Ukrainian State Scientific Research Institute of Refractories; a formula for calculating the static modulus of elasticity is derived and the temperature dependence of the modulus and bending strength is plotted. The molding method, treatment temperature, static modulus of elasticity, and bending strength of three types of ceramics with MgO and Y₂O₃ stabilizing additions are summarized. An abnormal dependence of the static modulus of elasticity of partially stabilized ZrO₂ ceramics within a 20-1,200°C range is established and attributed to the characteristics of ZrO₂ phase transitions under static loading. It is shown that the presence of a peak on the elasticity modulus curve of Y₂O₃-stabilized ceramics combined with its virtually constant bending strength makes this ceramics promising for use as a structural material. A decrease in the elasticity modulus and bending strength at temperatures above 1,000°C is attributed to the decreasing role of martensitic transformation in zirconium dioxide induced by the mechanical stresses in the monoclinic-to-tetragonal phase transition area as well as an increase in the plastic strain contribution. Figures 1; tables 1; references 9: 4 Russian, 5 Western.

Heat Insulating Rubber for Dry Binder Grinding Ball Mill Lining

927D0193E Moscow OGNEUPORY in Russian
No 6, Jun 92 pp 24-26

[Article by N.M. Shevchenko, G.P. Sheludko, N.Ya. Kuzmenko, Dnepropetrovsk Chemical Engineering Institute; UDC 621.926.5:66.043.1]

[Abstract] The high energy demand and noise level and the danger to occupational safety resulting from the use of ball mills with steel wear-resistant elements, which protect the balls from abrasion, prompted a study aimed at replacing the steel elements with rubber lining in ball mills for dry grinding of binders. The requirements imposed on such rubber lining are formulated, and the results of an investigation of the behavior of the most important characteristics of lining rubber, i.e., wear, hardness, strength, and elongation, during its operation in dry ball mills is discussed. The plasticity, elasticity, hardness, tensile strength, rupture strength, elongation, tearing strength, and thermal aging of the SKN-26M+SKD and SKEPT-40+Nairit-A rubber mixtures with and without additions are summarized, and the lining wear with and without organosilicon additions is plotted. An analysis of the rubber lining surface shows that wear occurs in it by a special mechanism, which is different from that of friction, abrasive, and fatigue wear. The study also indicates that the rubber lining service life may be extended by using such modifying additives as organosilicon compounds which are capable of retarding the onset of oxidation processes which usually develop in polymer compositions at high temperatures and can delay the transition of a less intensive impact-fatigue wear to a more intensive impact-abrasive wear. Figures 4; tables 1; references 8.

Dolomite-Dunite Mixture as Fettling Material for Steelmaking Furnaces

927D0193F Moscow OGNEUPORY in Russian,
No 6, Jun 92 pp 32-33

[Article by G.I. Antonov, V.P. Nedosvitii, A.S. Kulik, O.S. Kladko, G.N. Shcherbenko, Ukrainian State Scientific Research Institute of Refractories; UDC 666.762.38-492.2:669.183.211.32]

[Abstract] The suitability of forsterite-containing materials, e.g., dunites mixed with dolomites, as a fettling material for steelmaking furnaces is investigated due to shortages of not only periclase, but also dolomite powders. The comparative composition and refractoriness of dolomite-dunite and periclase-dunite mixtures and the mass proportion of the initial material and mixture components and their fraction composition are summarized, and the results of dolomite-dunite mixture tests at the Makeyevka, Krivoy Rog, and Kommunarsk integrated iron and steel works are presented. The technical requirements imposed on the SDD-30, SDD-32, and SDD-34 fettling composition mixture properties are formulated. The tests confirm the possibility of using the dolomite-dunite mixture as a fettling material and the relevant mixture specifications (TU 14-8-618-90) are adopted. The tests carried out in 250-650 ton furnaces did not reveal any difference in the service properties of the mixture. Commercial production of the dolomite-dunite mixtures is underway at the Nikitovskiy Dolomite Plant (NDZ) and Seversk Dolomite Combine (SDK). Tables 4.

Structure and Phase Composition of Rammed Lining and Channel Fouling Products of Magnetodynamic Aluminum Alloy Meters

927D0193G Moscow OGNEUPORY in Russian
No 6, Jun 92 pp 33-35

[Article by A.V. Kosinskaya, Zh.D. Bogatyreva, IPL at the Ukrainian Academy of Sciences; UDC 666.762.3:621.365.55.036.53]

[Abstract] Frequent stoppages of the MDN-2 submerged-resistor induction furnace operation with tamped lining prompted an investigation of the phase composition and structure of the tamped lining and E-shaped channel fouling products in the MDN-6A-0.16 unit used for automatic metering of aluminum and zinc alloys in casting machines. The lining material transformations in contact with aluminum and the structure and

phase composition of the skull forming in the channel are examined. An analysis of the findings makes it possible to speculate that the fouling process occurs in two stages: In the first, the lining components come into contact with Al due to wetting and spreading, so the material penetrates the lining pores and microcracks under the effect of capillary forces and external factors. The impregnation process is enhanced by the chemical reaction between the metal and the refractory binder. At the same time, the nonmetallic Al_2O_3 particles interact with the periclase, forming aluminum spinel which becomes cakes with the products of the aluminum + binder reaction. Thus, corrosion and erosion processes are dominant in the rammed lining failure. These findings make it possible to suggest a number of recommendations for increasing the serviceability of MDN-6 lining. Figures 3; references 4.

Numerical Modeling of Powder Compacting Utilizing an Axisymmetrical Impact

927D0177A Kiev POROSHKOVAYA METALLURGIYA
in Russian No 4, Apr 92 pp 11-16

[Article by V. A. Gorelskiy and S. A. Zelepuhin, Institute of Structural Macrokinetics at the Tomsk Affiliate of the Russian Academy of Sciences; UDC 621.762]

[Abstract] The finite elements method was used to study how steel and ceramic powders with different initial porosities are affected when placed in steel capsules and subjected to high-speed axisymmetrical compacting. The system of equations used describes the dynamic adiabatic motion of a compressed material, accounts for variable porosity, and consists of equations for continuity, motion, energy, and change in specific porosity. Chronograms were calculated to depict the impact absorbed by the steel capsules after 3 and 20 μ s. Impact speed was 1,000 m/s. Graphs showing change in powder porosity and temperature along the axis of symmetry, change in the internal and free energy of the powders, change in the kinetic and internal energy of the capsule as a whole, and change in the ratio of shear deformation energy to internal energy in the powders and capsules during impact were also constructed. The data show that the greatest differences in powder behavior occur during the initial stages of compacting. Higher temperatures are associated with ceramic powders having the same porosity as their steel counterparts. The radial, wave-like flow of the lower part of the capsule greatly affects the initial stage of impact. Because this process is characterized by high pressures and temperatures and intensive shear deformations, it is suitable for the shock-wave activation of powders and, hence, for the synthesis of new types of materials. Figures 4; references 13: 9 Russian, 4 Western.

Use of Hydrostatic Pressure of up to Five GPa To Compact Tungsten Powders of Various Dispersity

927D0177B Kiev POROSHKOVAYA METALLURGIYA
in Russian No 4, Apr 92 pp 16-20

[Article by V. P. Filonenko, L. G. Khvostantsev, R. Kh. Bagramov, L. I. Trusov, and V. I. Novikov, Institute of High Pressure Physics of the Russian Academy of Sciences, Troitsk; UDC 621.762]

[Abstract] The compaction of ultradispersed (0.02-0.1 μ m), submicronic (0.1-0.5 μ m), and micronic (3-8 μ) tungsten powders at hydrostatic pressures up to five GPa was studied to determine the compaction mechanism(s) that predominate for each particular type of powder. The compacting was done in a high-pressure "toroid"-type chamber. The powders were poured into an elastic casing and placed in a teflon vessel filled with a mixture of water and glycerine. Pressure in the vessel was controlled by monitoring the electrical resistance of a manganin sensor to within +0.05 GPa. The compacts were hydrostatically weighed to determine their density. Particle quality was assessed from the halfwidth of the diffraction

peak (321). Before compacting, some of the powder samples were reduction annealed to see how this treatment affected the compacting process. Data on compact density and particle imperfection showed that the predominant mechanism in ultradispersed powder compaction is mutual particle slip. Compact density was greatly increased when the ultradispersed powders were reduction annealed prior to compacting, as this reduced friction between particles. As particle size increases, plastic deformation plays an increasingly important role in compact density, whereas reduction annealing plays an increasingly less important role. With the submicronic powders, mutual slip was the predominant mechanism during the initial stage of compacting, with plastic deformation taking over in the latter stages. Compacting effectiveness in the submicronic powders was enhanced by adding a more plastic component, such as nickel. Figures 2; references 7: 6 Russian, 1 Western.

Studying the Sintering Process in the I_2O_3 -CuO System

927D0177C Kiev POROSHKOVAYA METALLURGIYA
in Russian No 4, Apr 92 pp 21-24

[Article by Yu. I. Boyko, Yu. I. Klinchuk, and V. P. Sukhomlin, University of Kharkov; UDC 621.762]

[Abstract] The kinetics and substance transfer mechanism at various stages of sintering were studied in the I_2O_3 -CuO system. Compacts were made from powders of the two respective substances thoroughly mixed in a molar ratio of 1 : 2 and in a ratio that was not quite stereometric. Cylindrical compacts 8 mm in diameter and three mm high were made by applying a pressure of 300 MPa in one direction. During sintering and isothermal annealing in an oxygen stream, compact dilatation was directly measured using a KM-8 cathetometer to within +0.05 percent. The dilatation measurements showed that compact size increased about 5 percent during the initial stage of the sintering process, and that compact "growth" was triggered by the formation of a new phase, $I_2Cu_2O_5$, as well as by diffusion homogenization characterized by unequal partial diffusion coefficients for the mutually-diffusing ions. During the initial stage of the sintering process, the critical role is played by the heterodiffusion process, which is characterized by the preferential diffusion of the copper ion into the I_2O_3 particle via the layer of $I_2Cu_2O_5$ being formed. In this system, substance transfer is controlled by oxygen ion diffusion, and diffusion homogenization is controlled by copper ion diffusion. Figures 2, references 8: 6 Russian, 2 Western.

Hot-Pressed Cupreous Powder Steels

927D0177D Kiev POROSHKOVAYA METALLURGIYA
in Russian No 4, Apr 92 pp 25-28

[Article by S. G. Napara-Volgina, Institute of Applied Materials Science, Ukrainian Academy of Sciences, Kiev; UDC 621.762]

[Abstract] Hot-pressed powder steels with various concentrations of copper and carbon were studied to determine optimal composition, properties, and pressing conditions. First, it was necessary to find out how a copper concentration of 2-8 percent would affect the mechanical properties of steels containing 0.01-0.02 percent carbon. Specimens 10 x 10 x 55 mm were made from a mixture of PZhR3 atomized iron powder and PMS-2 electrolytic copper powder pressed at 1100-1150°C, pre-sintered at 950-1000°C, and aged at 450°C. Tensile-test specimens were then machined from the hot-pressed specimens. Optimal copper content was found to be 4-5 percent. In the next part of the study, specimens containing 5 percent copper and various carbon concentrations were pressed at either 1130-1180°C or 800-850°C, quenched from 950°C, and tempered at 450°C or 550°C. It was found that carbon content had little effect on the strength of specimens pressed at the higher temperatures. This was attributed to the natural aging that occurs after pressing at these temperatures. On the other hand, specimens pressed in the lower temperature range had much lower strength values after pressing, but this was remedied by artificial aging induced by quenching and tempering the specimens at 450°C. When specimens containing up to 0.30-0.35 percent carbon were pressed at the higher temperatures, quenched, and tempered at 550°C, the natural aging effect was completely destroyed and strength dropped nearly two-fold. Under the same conditions, specimens with more than 0.30-0.35 percent carbon increased in strength, as would be expected. It was then determined that the maximum amount of carbon that could be added to the specimens without disrupting the natural aging process was 0.3 percent; higher carbon concentrations would dictate further heat treatment in order to optimize mechanical properties. Optimal strength (900-1050 MPa) and elongation (10-12 percent) were found in steel with 5 percent copper and 0.2-0.3 percent carbon. Figures 4, references 2: Russian.

Optimizing the Composition of the Nickel Binder in WC-Ni Hard Alloys by Alloying the Binder With Elements From Groups IV-VI

927D0177F Kiev POROSHOVAYA METALLURGIYA
in Russian No 4, Apr 92 pp 31-37

[Article by R. F. Cheburayeva, I. N. Chaporova, Yu. F. Rudakov, and T. I. Krasina, All-Union Scientific Research Institute of Hard Alloys, Moscow; UDC 669.018.25]

[Abstract] A mathematically designed experiment was used to determine whether the hardness of the nickel binder in WC-Ni hard alloys could be increased to equal that of a cobalt binder without compromising strength by alloying the binder with molybdenum, tungsten or monocarbides (TiC, HfC, VC, NbC, TaC, or Cr₃C₂). The concentration of the alloying elements was kept below their saturation point in order to prevent the formation of phases that would reduce alloy strength. Powder

metallurgy was used to make compacts that were presintered at 670-700°C in a stream of hydrogen in order to remove the plasticizer and reduce the oxides. Final sintering was done in a vacuum at 1280-1300°C for four hours, after which the specimens were quenched to preserve the requisite alloying element composition. The specimens were then machined to prepare them for mechanical testing. After machining, the specimens were annealed at 1250°C to remove stress. The specimens were then examined to determine their chemical composition, microstructure, phase composition, lattice spacing in the nickel phase, microhardness, and tensile strength. The data obtained were processed on a Mir-1 computer using linear regression analysis. Evidently, in order for the nickel binder to attain a hardness that approximates that of a cobalt binder without sacrificing strength, it must be alloyed with a combination of molybdenum and chromium, niobium, and hafnium carbides. A search for an optimal combination of properties yielded: 4000 MPa for hardness, 500 MPa for strength, 264 MPa for the yield point, and 14.7 percent for ductility. Two alloy groups were found to have optimal compositions: Ni-WC-Mo-HfC-NbC, which is comparable in strength and hardness to (Co)W,C, and Ni-WC-Mo-HfC-Cr₃C₂, which is somewhat superior to it. Tables 6; references 8: 2 Russian, 6 Western.

Shrinkage and Dimensional Accuracy in Products Made of Sintered Titanium Alloy

927D0177K Kiev POROSHOVAYA METALLURGIYA
in Russian No 4, Apr 92 pp 97-99

[Article by V. N. Kazakov, V. I. Kryukov, and N. P. Morozov, Kuybyshev Aviation Institute; UDC 621.762]

[Abstract] Shrinkage in specimens sintered from titanium hydride was studied. The ring-shaped specimens were compacted at 1170-1270 MPa from powders of three different fractions and from a mixture consisting of equal portions of these powders. At least 200 specimens were made from each type of powder and from the mixture. At least 150 specimens of equal density (4,200 + 100 kg/cu m) were selected from each batch. The compacts were sintered at 1300°C in a .067-Pa vacuum for two to four hours in order to keep shrinkage to a minimum and to preserve near-net-shape dimensional tolerances. A micrometer was used to measure specimen size and shrinkage, and the results statistically analyzed. The arithmetic mean value for shrinkage ranged from 0.52 to 0.67 percent, with higher shrinkage values associated with smaller particle size and longer sintering times. When the standard deviation for shrinkage values is factored in, shrinkage can range from 40 to 60 percent of the mean. Therefore, statistical methods that account for this disparity must be used in order to accurately estimate shrinkage and dimensional tolerances and to design compacting and sintering equipment. A specific approach to improving dimensional tolerances is recommended. Tables 1, references 2: Russian.

Generation of Vacancies Stimulated by the Chemical Etching of a Crystal Surface

927D0182E Moscow *POVERKHНОST: FIZIKA, KHIMIYA, MEKHANIKA* in Russian No 10, Oct 92 pp 122-127

[Article by A. G. Italyantsev, Institute of Problems in Microelectronics and Especially Pure Metals Technology of the USSR Academy of Sciences, Chernogolovka; UDC 536]

[Abstract] The generation of non-equilibrium vacancies stimulated by the chemical reaction induced by etching a crystal, specifically the formation of point defects in both single-atom and complex crystals without disturbing their stereochemistry, is studied. The case at hand differs from Shottky's classic model in that 1) it pertains to the generation of non-equilibrium V, when, under specific conditions, a chemical reaction becomes a kind of "pump" that draws the V from the surface into the interior of the crystal and 2) here, the formation of V on the crystal surface and their migration into the interior is brought about by the rate at which the atoms are etched in the normal direction and by crystal temperature, and these two parameters can vary widely and independently of one another. In order for the process of chemical etching to be accompanied by the injection of the vacancies into the interior of the near-surface layers of a crystal, several criteria must be satisfied: 1) the etching must be direct, i.e., it must entail direct dissolution of the atoms in the solvent without the formation of a new intermediate phase that is subsequently dissolved; 2) the crystal must meet certain criteria for the accuracy of its surface orientation relative to the singular faces and for structural defect density so that the atomic spacing on the crystal surface exceeds a specified value; 3) there is a limit to the micro- and macro-etching rates; and 4) the lower temperature threshold is linked to a specific ratio between the etching rate and vacancy diffusion, and the maximum temperature is dictated by the temperature at which a smooth atomic surface transforms spontaneously into a rough atomic surface. Vacancies injected into the near-surface layers can enter into a quasichemical reaction with various types of crystal defects. Figures 3; references 15: 11 Russian, 4 Western.

High-Vacuum Thermal Cleaning of Si Surfaces With a Protective Oxide Film

927D0182J Moscow *POVERKHНОST: FIZIKA, KHIMIYA, MEKHANIKA* in Russian No 10, Oct 92 pp 154-157

[Article by V. A. Perevoshchikov, V. D. Skupov, V. G. Shengurov, and L. Ye. Nikolayeva, Scientific Research Institute of Applied Physics at Novgorod State University; UDC 621.794:546.681.191.1]

[Abstract] The use of oxide solutions to pre-clean silicon substrates was studied to determine the effect on the annealing temperature in vacuum and on the structural perfection of silicon layers grown on these substrates. The experiments were carried out on rectangular wafers of KDB-20 silicon with a working surface orientation of 100. The specimens were prepared in a standard manner and treated in either an ammonia-peroxide or a nitric acid-based solution to form a protective oxide film, rinsed in twice-distilled water and dried. After passivation, the wafers were placed in a growing chamber and heated to 700-1300° for 15-30 minutes by passing a current through them in a 10⁻⁷-torr vacuum. Epitaxial silicon layers about 3 μm thick were grown on the cleaned substrates at a rate of 3.5 μm/h at a substrate temperature of 600-800°, using wafers of KDB-0.1 Si heated to 1380° by passing current directly through them as the source of the silicon atom and alloying element (boron) vapors. Substrate and layer structure was studied electronographically and metallographically. It was found that the growth of the monocrystalline silicon layers depends greatly on the desorption properties of the protective oxide film. By using the nitric-acid based solution, the annealing temperature can be lowered by 400-500° in comparison with wafers passivated in the more commonly used ammonia-peroxide solution. The use of the nitric acid-based solution also promotes the formation of structurally defect-free epitaxial layers even at a relatively low negative pressure. In this case, the stacking fault density of the silicon layers grown on the cleaned surfaces was < or = 10² cm⁻². Figures 1, tables 1; references 5: 3 Western, 2 Russian.

Treatments**JPRS-UMS-92-012****12 August 1992** **α -Ti Straining Temperature Manipulation.
Mechanical and Substructural Aspects**

927D0191B Kiev METALLOFIZIKA in Russian
Vol 14 No 1, Jan 92 pp 9-15

[Article by A.R. Smirnov, V.A. Moskalenko, Low-Temperature Engineering Physics Institute at the Ukrainian Academy of Sciences, Kharkov; UDC 539.2]

[Abstract] Various version of two-stage straining with a temperature change at 4.1, 77, and 293K are considered from the viewpoint of establishing the effect of preliminary plastic deformation at a T_1 temperature on the level of straining stress at a T_2 temperature. To this end, the behavior of the mechanical properties of α -Ti is investigated and compared to the dislocation substructure transformations; technically pure 0.1 mm thick titanium foil is used in the study. A check experiment is also conducted in order to ensure that the phenomena related not to the Ti prestraining proper but simply to the load relieving procedure or substructural changes during the heating or cooling do not affect the outcome of the mechanical tests. Tensile diagrams with a straining temperature change from 77 to 293K and from 293 to 77K are plotted. The findings partially confirm the theoretical prediction that in a sample deformed by 10 percent at 293K and again by 2 percent at 4.2K, the specific volume of material per reorientation strip (PP) is approximately equal to 27 percent whereas in the same sample not subjected to the subsequent low-temperature straining, this figures reaches 55 percent. The tests show that substructure formed during the prestraining at 293K does not inhibit the low-temperature twin propagation and the low-temperature substructures highly fractured with twins are more stable to subsequent straining at 293K than the strip substructures are to low-temperature straining. Figures 4; references 5: 4 Russian, 1 Western.

Effect of Dynamic Straining on Steel 30KhN4M Microstructure Kinetics

927D0191C Kiev METALLOFIZIKA in Russian
Vol 14 No 1, Jan 92 pp 21-27

[Article by S.A. Atroshenko, S.A. Gladyshev, Yu.I. Meshcheryakov, St. Petersburg Branch of the Mechanical Engineering Institute at Russia's Academy of Sciences and All-Union Steel Scientific Research Institute, Moscow; UDC 539.374]

[Abstract] The effect of heat pretreatment—water quenching at 900°C with subsequent tempering at a 200, 550, 600, and 650°C temperature during three hours—on the microstructure behavior of steel 30KhN4M during dynamic straining is investigated. To this end, the pretreated samples are subjected to impact loading whereby flat targets are loaded by a compressed-air-and-gas gun with a 37 mm caliber at a 200-400 m/s velocity. The microstructure of the transverse metallographic sections after pickling is examined under a Neophot-32 optical microscope and a Camscan scanning electron microscope. The microhardness (Knoop) of the

strained samples is measured in a Buehler-MetAg instrument at a 100 g load while the X-ray diffraction analysis is carried out by a DRON-2 diffractometer in FeK_{α} radiation. The behavior of the grain size, carbides, and microhardness as a function of the tempering temperature, the dependence of the α -phase lattice parameters and α -phase tetragonality before and after impact loading on the tempering temperature, the dependence of the lattice cell parameter on the straining rate, and the dependence of the lattice cell parameter on the straining temperature are plotted. An analysis shows that the carbide phase dispersivity has a dominant effect on microhardness at a straining rate of under 320 m/s while the grain size—at rates above 320 m/s; the greatest microhardness is observed in steel tempered at 200°C at 320 m/s and steel tempered at 650°C at 324 m/s; and the greatest hardening effect is obtained in steel with the most uniform structure tempered at 650°C. An abnormal carbide growth in steel under impact loading and the rotational straining and fracture mechanism of steel tempered at high temperatures are noted. The authors are grateful to V.B. Vasilkov and A.I. Chernyshenko for helping with the tests. Figures 5; tables 1; references 4.

Microcrack Curing in Pulse Strained Mo During Annealing

927D0191D Kiev METALLOFIZIKA in Russian
Vol 14 No 1, Jan 92 pp 28-33

[Article by M.N. Belyakova, Yu.V. Korniyushin, L.N. Larikov, P.V. Mudruk, Physics of Metals Institute at the Ukrainian Academy of Sciences, Kiev; UDC 539.219.2]

[Abstract] The curing of surface microcracks developing in molybdenum single crystals after pulse loading is investigated. To this end, 99.999 percent pure Mo single crystals shaped as a 5x8x10 mm bar are compressed along the <111> axis at a 10^2 s⁻¹ pulse rate; as a result, microcracks formed on the lateral faces which did not come into contact with the loading tool. The microcrack curing, starting with the crack apex, is determined after isothermal annealing within a 1,070-1,870K temperature range using scanning electron and optical microscopy. The study reveals that in pulse strained Mo single crystals, the surface microcracks are cured at an abnormally low annealing temperature of $0.37T_{melting}$, attesting to the fact that curing cannot be attributed at such temperatures to the surface diffusion mechanism. It is speculated that the movement of the dislocations remaining in the material plays a dominant role in the microcrack curing process. This curing by the dislocation motion mechanism through mass transfer may indeed be realized in pulse loaded crystals since a high level of internal stresses and a large number of excess point defects, both vacancies and interstitial atoms, and dislocations develop under such straining. It is shown that the curing rate is accelerated due to the dislocation structure inhomogeneity. Figures 4; references 11: 9 Russian, 2 Western.

Characteristics of Fe and Ni Mass Transfer in Metals During Propagation of Pulse Radiation-Generated Shock Waves

927D0191F Kiev METALLOFIZIKA in Russian
Vol 14 No 1, Jan 92 pp 46-49

[Article by A. Dubik, L.O. Zvorykin, Ya. Ovsik, V.M. Falchenko, A.V. Filatov, Physics of Metals Institute at the Ukrainian Academy of Sciences, Kiev; UDC 669.127]

[Abstract] The possibility of pulse laser treatment of metals in order to stimulate shock wave transmission with a short shock pulse duration (1 ns) is investigated. To this end, Cu, Fe, and VT-4 alloy samples ground and polished to a 0.1 μm roughness, then coated with $^{55}, ^{59}\text{Fe}$ or ^{63}Ni and covered with a protective Cu layer are exposed to pulse laser radiation; the Cu layer is applied to protect the mass transfer zone formed during the loading from erosion processes and heating. The samples are then studied by the tracer method using the autoradiography and layer-by-layer radiographic analysis as well as electron and optical metallography and X-ray diffraction microanalysis. The dependence of the Ni penetration depth in Cu, Fe, and the VT-4 alloy and Fe penetration depth in the VT-4 alloy on the laser radiation density is plotted and the Ni and Fe mass transfer depth in Cu, Ni, and the VT-4 alloy and the diameters of the craters formed by 1 ns pulse laser radiation of varying intensity are summarized. An analysis of the findings shows that the mass transfer in metals and alloys stimulated by high-density radiation occurs primarily in accordance with the general patterns typical of other types of loading generating shock waves in metals provided that the erosion processes are not intensive and the temperature variations are insignificant. Figures 2; tables 1; references 4.

Effect of Proton Irradiation on Electric Charge Formation in Mailar and Teflon Films

927D0192B Moscow FIZIKA I KHIMIYA OBRABOTKI MATERIALOV in Russian
No 3, May-Jun 92 pp 12-15

[Article by V.V. Gromov, G.M. Sessler, R. Doersam, Moscow and Germany; UDC 539.2:539.12.04.541.64:537.311]

[Abstract] The near-surface layer charging phenomenon in insulators irradiated with heavy charged particles due to effective particle deceleration by the first layers of the substance is discussed, and the electric charge distribution in mailar and teflon films widely used in space technology under irradiation with protons at a 0.23 and 0.8 eV energy, which corresponds to the proton energy in the solar wind and determines the principal heavy particle irradiation-induced effects in spacecraft materials, is investigated. To this end, the films are irradiated in a vacuum under a 1-15 s exposure. Roughly one hour after irradiation, the sign and magnitude of the external electric field created by the space charge of the implanted

protons on the film surface and the space charge distribution in the sample depth are measured by electrometry and acoustic probing, respectively. The density, dielectric permittivity, resistivity, and ultrasound speed in the materials are summarized, and the dependence of the surface potential on the irradiation time is plotted. The study is carried out in Darmstadt in a unit with a spatial resolution of close to one μm . An analysis of the findings reveals an extremely irregular charge distribution in the bulk of the film which is attributed to the redistribution of the charge carriers appearing under proton irradiation. The positive charge localization coordinate is quite consistent with the proton free path length in the materials under study. Figures 3; tables 1; references 7: 4 Russian, 3 Western.

High-Dose Fe Ion Implantation at Room Temperature

927D0192C Moscow FIZIKA I KHIMIYA OBRABOTKI MATERIALOV in Russian, No 3, May-Jun 92 pp 16-19

[Article by E.M. Diasamidze, A.N. Kalinin, Sukhumi; UDC 539.213.621.382]

[Abstract] The importance of iron—the basic element of most structural materials—for radiation materials science is noted, and a Fe-Nb⁺ implanted system and published experimental data on Fe-B⁺, Fe-Si⁺, and Fe-P⁺ are considered from the viewpoint of configurational and thermal models of structural and phase transitions; in addition, an Nb-Fe⁺ implanted system is discussed; 80 nm Fe films are produced by evaporating armco iron and tungsten filament onto a cleavage of a rock salt crystal; 80 nm Nb films are produced by direct evaporation of a Nb filament. The samples are analyzed in an ER-100M electron transmission diffraction analyzer at a 100 keV electron energy. The critical doses of structural transformations under ionic Fe implantation, i.e., the dose and the energy as well as the implantation dose limit, critical amorphization dose in the thermal model, intermetallic compound development criterion, and critical dose of structural transformation, are summarized. The study shows that a Laves phase forms under Fe irradiation with Nb⁺ while the film is totally amorphized under Nb irradiation with Fe⁺. Under irradiation with B⁺, only the configurational amorphization model is in effect even though Hegg's criterion is equal to 0.65 since the thermal peak virtually does not form. During Nb irradiation with Fe⁺ ions, amorphization occurs at a dose some ten times lower than the critical amorphization dose in the thermal model. The authors are grateful to G.V. Afanasyev and N.M. Kutsiya for assistance. Tables 1; references 13: 7 Russian, 6 Western.

Age-Hardened Nickel Alloy Behavior Under Radiative Heat Treatment

927D0192D Moscow FIZIKA I KHIMIYA OBRABOTKI MATERIALOV in Russian No 3, May-Jun 92 pp 20-27

[Article by N.M. Zaytseva, I.I. Volodina, V.A. Kulikov, Tomsk; UDC 669.245:539.1.043]

Treatments

JPRS-UMS-92-012
12 August 1992

[Abstract] The effect of high-energy ionizing radiation flux interaction with matter is examined from the viewpoint of space research and fusion energy applications, and the effect of the resulting structural transformations and the disperse phase on the properties of the materials are discussed. The effect of γ -quanta irradiation from a ^{60}Co source at a 1.27 MeV energy on the structural transformations in age-hardened nickel alloys both before and after high-temperature annealing at 1,573K in an argon medium is investigated experimentally. To this end, two nickel alloys containing roughly 2.5 percent of the disperse phase by volume are examined. The kinetics of structural changes after irradiation with $2.4 \cdot 10^5$ and $5 \cdot 10^7$ R at 313K in the air are estimated on the basis of Debye's characteristic temperature. The particle size distribution in relation to the total number of measured particles, the number of particles in irradiated alloys per unit of area as a function of the subsequent annealing duration, and the mean number of particles in irradiated alloys as a function of the subsequent annealing duration are plotted and the X-ray phase analysis data on the disperse phase are summarized. The number of particles per unit of area increases and the mean particle size changes nonmonotonically. The findings demonstrate that the structure of age-hardened nickel alloys changes both under irradiation with gamma-quanta and during the subsequent annealing while the structural and phase transformation are due to the three competing processes occurring in the materials under exposure: particle dissolution, precipitation of new particles, and coalescence. It is speculated that the postirradiation relaxation of the age-hardened alloys is determined by the spontaneous formation and breakdown of some new dissipative structures leading to the alloy component redistribution. Figures 7; tables 1; references 13: 9 Russian, 4 Western.

Phase Formation in V_2O_5 Single Crystals Under Irradiation With Electrons of Varying Energy

927D0192E Moscow FIZIKA I KHIMIYA OBRABOTKI MATERIALOV in Russian, No 3, May-Jun 92 pp 28-33

[Article by L.M. Kryukova, Ye.V. Uspenskaya, Moscow; UDC 537.533.35.7]

[Abstract] A shortage of sound studies in the field of radiation physics of solids and the kinetics of phase transitions in materials under external factors, such as irradiation, are noted, and the sequence and kinetics of phase transformations in the V_2O_5 higher oxide under the effect of irradiation with electrons of varying energy are investigated within an 80-150 keV range. It is stressed that transition metal oxides are a good model material since phase transitions can be observed in them directly under a microscope. Single crystals grown at the Crystallography Institute are used in the experiment; an *in situ* study is made under a Tesla BS-540 transmission electron microscope at an 80-120 kV accelerating voltage and under a JEM-100 electron microscope at a 1,000 kV accelerating voltage. The samples are irradiated with electrons at a 10-40 keV energy under a JSM-35 scanning

electron microscope; the findings are processed under He-Ne laser radiation. The experiment shows that the phase formation mechanism depends on the electron energy and that irradiation with 80-250 keV electrons induces the formation of linear and planar split defects with subsequent phase transitions by the high-rate spinodal decay mechanism. The effect of >400 keV electrons causes a direct $\text{V}_2\text{O}_5 \rightarrow \text{VO}$ transition occurring by the nucleation mechanism. At a certain field strength, the oxide loses coherence and the crystalline grain growth terminates. Figures 4; references 7: 4 Russian, 3 Western.

Effect of Pulse Laser Radiation on Wrought Aluminum Alloys

927D0192F Moscow FIZIKA I KHIMIYA OBRABOTKI MATERIALOV in Russian No 3, May-Jun 92 pp 34-37

[Article by S.A. Maslyayev, V.I. Neverov, V.N. Pimenov, I.P. Sasnovskaya, Moscow; UDC 669.71:535.241]

[Abstract] Intensive development and wide-ranging implementation of laser heat treatment of materials prompted an investigation for the processes of microstructure formation in commercial alloys under the effect of laser radiation (LI); the behavior of wrought aluminum alloys under the effect of pulse laser radiation (ILI) is investigated. To this end, samples from the D19 duralumin, AK4 high-temperature, V95 high-strength, and 1420 especially light "perspiring" alloys are examined. The samples are irradiated in a GOS-1001 unit in a free lasing mode with $0.7 \cdot 10^{-3}$ pulses at a $5 \cdot 10^5 \text{ W/cm}^2$ density. The sample structure is studied by optical and scanning electron microscopy. The HV microhardness and structure of the alloy samples before and after laser irradiation are summarized. An analysis of the experimental results shows that the surface and near-surface layers of wrought aluminum alloys irradiated with millisecond pulses in a free lasing mode melt and harden; these processes are accompanied by an α -solution grain refinement, secondary hardening phase dissolution in the melt, a decrease in microhardness, and cracking. Intense gas liberation in the liquid phase is noted in the 1420 alloy; this process is attributed to the lithium hydride and hydrocarbonate decay. Figures 2; tables 1; references 12.

Structural Changes in Encapsulated Polysilicon Layers Under Effect of Scanning Laser Radiation

927D0192G Moscow FIZIKA I KHIMIYA OBRABOTKI MATERIALOV in Russian No 3, May-Jun 92 pp 38-43

[Article by A.A. Druzhinin, I.T. Kogut, V.T. Kostur, O.M. Lyba, T.V. Rodionova, Lvov; UDC 621.315.592]

[Abstract] The behavior of polycrystalline silicon layers applied to the surface of a silicon wafer cover with silicon dioxide and formed by the vapor phase chemical deposition method under the effect of laser irradiation is discussed from the viewpoint of semiconductor applications, and the structure and morphology of polysilicon layers encapsulated during the recrystallization process under scanning laser radiation are investigated. Individual types of surface defects are examined with the help of optical and scanning electron microscopy (SEM). Thermally oxidized Si wafers with a (100) orientation and a 1.0 μm SiO_2 thickness are used as the source materials. Then a 0.5-0.6 μm thick polysilicon layers are deposited by the low pressure LPCVD method; the initial grain size is 40 μm . After that the entire structure is covered with a 0.7 μm silicon dioxide layer. The wafers are exposed to CW scanning YAG:Nd⁺ laser radiation in the air at a 20 mm/s rate at a 600°C temperature; for the purpose of metallographic studies, the wafers are pickled in an HF : $\text{HNO}_3 = 1 : 3$ mixture. The findings show that the encapsulating coat greatly stabilizes the grain growth, lowers the mass transfer, and helps to form a clear (100) texture under laser irradiation; chevron grain boundary and subboundary nets, twins, lattice packing flaws, individual dislocations, and dislocation clusters are the main recrystallization layer defects after a scanning laser radiation exposure. It is shown that under optimum laser treatment conditions, the recrystallized layers consist of quasisingle crystals with 15x100 μm crystal grains. Figures 4; references 7: 3 Russian, 4 Western.

Effect of Laser Radiation on CdTe Optical and Mechanical Properties

927D0192H Moscow FIZIKA I KHIMIYA OBRABOTKI MATERIALOV in Russian No 3, May-Jun 92 pp 44-46

[Article by A.V. Savitskiy, P.P. Beysuk, I.V. Budzulyak, A.N. Lyakhovich, K.S. Ulyanitskiy, Chernovtsi; UDC 621.315.592]

[Abstract] Limited applications of crystalline cadmium telluride in the national economy due to its poor mechanical properties despite its 65-68 percent non-structural transmission and the lack of data on the effect of irradiation on the mechanical properties of CdTe crystals prompted a physical and process behavior investigation of CdTe crystals in order to improve their mechanical strength. The study is carried out by the laser wafer treatment method whereby the treatment energy and duration are selected so as to ensure that the wafer surface is fused without heating the bulk of the sample. The crystals for the study are Bridgeman-grown from a close-to-stoichiometric melt under a low cadmium vapor pressure; the dislocation density in the initial samples is $2 \cdot 10^5 \text{ cm}^{-2}$. The polished samples are exposed to ruby and Nd laser radiation pulses at 1.81 and 1.7 eV, respectively, with a 1 s duration, leading to the development of craters. The transmission spectra of intrinsic and doped CdTe and the transmission spectra of CdTe wafers after laser treatment with and without subsequent

mechanical and chemical polishing are plotted. The study made it possible to establish the optimum conditions for nondestructive laser fusion conditions: a pulse energy density of 30-90 J/cm². After optimal treatment, the surface microhardness increases to 95-110 kg/cm² which is 1.75-1.9 times higher than that of untreated samples. After laser treatment, the surface transmittance drops, but this can be corrected by mechanical and chemical wafer treatment. Figures 3; references 2: 1 Russian, 1 Western.

Simulation of Cosmic Radiation Effect on Materials

927D0192I Moscow FIZIKA I KHIMIYA OBRABOTKI MATERIALOV in Russian No 3, May-Jun 92 pp 47-57

[Article by A.I. Akishin, I.B. Teplov (deceased), Moscow; UDC 621.315.3]

[Abstract] The effect of various external factors, primarily the cosmic radiation, on the materials in spacecraft (KA) in the circumterrestrial and interplanetary space, particularly communications and television satellites (ISZ) which must function stably in a geostationary orbit for a long period of time (up to 10 years) is reviewed on the basis of numerous published sources, both domestic and foreign, and the need to simulate the effect of cosmic radiation for improving spacecraft design is stressed. An energy diagram of corpuscular fluxes of various origins interacting with materials in space and in simulators, the dependence of the oxygen atom fluence bombarding the satellite surface on the orbit altitude and the rate of material ablation due to chemical atomization, the energy spectrum of the electric potential along the diameter of shaded and illuminated insulating satellite surface, and the energy spectrum of protons in the earth's Van Allen belt are plotted. The issues of flux interaction of atomic oxygen in the earth's ionosphere with satellite materials, geostationary satellite electrification, radiation strength of spacecraft materials, radiation effects of heavy nuclei, and the role of nuclear processes in the radiation strength of satellite equipment containing optical and semiconductor materials are addressed. Figures 11; tables 2; references 17: 12 Russian, 5 Western.

Effect of Polishing on Surface Properties of Glass

927D0192M Moscow FIZIKA I KHIMIYA OBRABOTKI MATERIALOV in Russian No 3, May-Jun 92 pp 99-104

[Article by N.N. Khomenko, S.Yu. Lysenko, Chernigov; UDC 666.1.037.3]

[Abstract] The effect of glass polishing, e.g., for subsequent electric field welding, on the chemical composition and mechanical properties of the glass surface is discussed, and the process of mechanical polishing and welding of the Pyrex glass (GOST 21400-75) is investigated. To this end, samples are polished after the grinding procedure which involves consecutive glass surface treatment with aqueous suspensions of the M40,

Treatments

JPRS-UMS-92-012
12 August 1992

M28, and M10 silicon carbide powders in steel grinders. The effect of specific polishing loads on the polishing quality is evaluated; the study shows that unit pressure has a positive effect on the surface quality. The surface roughness profiles of the Pyrex glass produced under various unit pressures, the dependence of the Pyrex glass surface microhardness measured by the indentation method on the unit polishing pressure, and the dependence of the welding current on the welding duration are

plotted and the weldability characteristics are estimated. An interrelation between the polishing and welding processes is established, and the effect of the roughness parameters on the welded joint strength is assessed; it is shown that the optimal clamping pressure during polishing is 1.5 g/mm^2 . The glass surface formed under these conditions has the maximum reactivity, i.e., the highest reaction rate and peak welding current. Figures 4; tables 5; references 7: 6 Russian, 1 Western.

Explosion Welding of Tubes to Tube Plates

927D0192N Moscow FIZIKA I KHIMIYA OBRABOTKI MATERIALOV in Russian No 3, May-Jun 92 pp 117-121

[Article by Yu.L. Alekseyev, L.I. Lepekhina, G.M. Smirnova, Volgodonsk; UDC 621.771.8]

[Abstract] Fastening of 16x2.5 mm dia. tubes from steel 1Kh2M to tube plates from steel 3 is investigated. The study is carried out using three types of blaster cartridges; two of these are charged with the 6ZhV ammonite with a 1-1.05 g/cm³ density and one—with the phlegmatized RDX with a 1 g/cm³ density. The cartridge shell is made from 0.4-0.5 mm thick polyethylene; the explosive charge (VV) is ignited in the cartridges by a DSh-A demolition cord section. The detonation rate and

the tube surface velocity are recorded by an S9-8 oscilloscope. The dependence of the maximum tube expansion on the initial clearance for the three types of cartridges and the dependence of the welded joint strength on the mounting clearance value are plotted. The tests demonstrate that a low detonation rate favorably affects the welded joint strength and that this strength also depends on the mounting clearance; the physical contact between the metals which ensures the high joint strength is attained due to the thermal processes occurring during the air compression in the mounting clearance. Optimal selection of this clearance makes it possible to leave a relatively thin link between the tubes in heat exchanger tube plates thus decreasing the overall dimensions of such heat exchangers and increasing their efficiency. Figures 7; references 2.

Alekseyevka Deposit Dolomites

*927D0193C Moscow OGNEUPORY in Russian
No 6, Jun 92 pp 16-19*

[Article by T.N. Dolgikh, A.K. Karklit, S.Yu. Kovaleva, L.L. Vanicheva, All-Russia Institute of Refractories; UDC 622.355.14]

[Abstract] The outcome of the additional prospecting of the deep-lying dolomite levels at the Alekseyevka deposit in Kokchetav oblast is described, and the results of earlier dolomite tests performed by the All-Russian Institute of Refractories are presented. It is noted that today Alekseyevka dolomite roasted in rotary kilns at 1,650-1,730°C is one of the best powders for making converter refractories as well as for use as a metallurgical fettling powder. Differential thermal analyses are carried out using four core samples taken from the deposit; the findings make it possible to determine that two samples belong to the DK-2 dolomite class according to the TU 14-2-232—77 specifications and the other two, to the DSM-1 class according to the OST 14 84—82 standard. The conclusion is drawn that a lime-periclase powder for converter refractories can be prepared from one sample in a rotary kiln by roasting at 1,720-1,750°C and from another—by roasting at 1,750°C, while certified DOM-1 metallurgical dolomite can be produced pursuant to the OST 14 85—82 standard from the remaining two samples by roasting in a rotary kiln at 1,700-1,720°C. The difficulty of commercial implementation of the joint roasting of burnt and raw finely ground dolomite is noted. It is shown that the dolomite baking can be enhanced by adding 2 percent of iron scale to dolomite lumps. Figures 3; tables 3; references 5.

Analysis of Chalgalovskiy Deposit Kaolin

*927D0193D Moscow OGNEUPORY in Russian
No 6, Jun 92 pp 19-21*

[Article by R.S. Shulyak, V.V. Primachenko, L.N. Zolotukhina, A.N. Zakovorotnyy, Ukrainian State Scientific Research Institute of Refractories and Amur Integrated Scientific Research Institute; UDC 622.361.2:666.762.1.001.4]

[Abstract] Kaolin from the Chalgalovskiy deposit in the Amur oblast is examined comprehensively in order to expand the raw material base of the refractories industry; a preliminary analysis shows that kaolin consists of kaolinite—fine scale-like particles aggregated into colorless clusters with a total refractive index of 1.557 +/- 0.003—and quartz with feldspar, muscovite, and halloysite additions. The chemical content, granulometric composition, and properties of kaolin are summarized, and the differential thermogravimetric analysis curves are plotted. The curves indicate that the mass loss within a 50-700°C temperature range reaches 5.5 percent which corresponds to a 60-65 percent kaolinite concentration; the granulometric study performed by Figurovskiy's method shows that unprocessed kaolin is quite rough (with 27.7 percent of particles smaller than 2 µm) and

oversanded (60.2 percent sand content) and has a density of 2.63 g/cm³. The dependence of the untreated and treated kaolin properties on the roasting temperature is plotted, and baking tests are carried out; a study of baked samples shows that the optimum roasting temperature of unprocessed kaolin is 1,500°C while the optimum enriched kaolin roasting temperature is 1,400°C. Chamotte from such kaolin is suitable for making refractory materials while chamotte from untreated oversanded roasted kaolin cannot be used for making refractories and must be enriched. Figures 2; tables 3; references 1.

Statute on Procedure for Mineral Licensing

*925D0601B Moscow KOMMERSANT in Russian
No 29, 13-20 Jul 92 p 4*

[“Statute: On the Procedure for Licensing the Use of Mineral Resources”]

[Text] On 15 July the Supreme Soviet of Russia approved the Statute on the Procedure for Licensing the Use of Mineral Resources, which concretizes the procedure for the use of mineral resources proclaimed in the Russian Federation law “On Mineral Resources” of 21 February 1992. In the opinion of experts, the statute introduces specificity into relations between the state and private entrepreneurs in the use of Russia's main hard currency resource—mineral resources. This specificity consists in that, in keeping with the document that has been adopted, state structures retain control over the extraction of mineral resources. In order to obtain licenses, entrepreneurs must maintain “good relations” with the state structures since the statute contains no objective criteria for issuing licenses.

...2. The state system for licensing the use of mineral resources

...2.2. Licenses are granted through the state licensing system, organized support for which is the responsibility of the State Committee for Geology of Russia and its territorial subdivisions.

2.3. The State Committee for Geology of Russia and its territorial subdivisions keep track of existing and newly discovered objects of licensing, prepare proposals concerning the procedure, time periods, and conditions for assimilating them or including them in the state reserve...

2.4. These proposals are coordinated with the Ministry of Economy and Financial Resources of the Russian Federation, the Ministry of Industry of the Russian Federation, the Ministry of Fuel and Energy of the Russian Federation, the Ministry of Health of the Russian Federation... the State Committee of the Russian Federation for Safe Work in Industry and Mining Supervision, and other state organs...

2.5. After terms are coordinated... the list of facilities proposed to be offered for use and the conditions for

offering them are determined in conjunction with the organ of the representative power of the republic of the Russian Federation, kray, oblast, or autonomous entity and the State Committee for Geology of Russia or its territorial subdivision...

2.6...The decision to grant (issue) licenses is made in conjunction with the organ of representative power... and the State Committee for Geology of Russia or its territorial subdivisions...

3. Sections of mineral resource areas granted for use

...3.2. The license specifies the boundaries of the section of mineral resource area granted, within which the work indicated on the license is permitted...

3.3. Sections of mineral resource areas are granted for use in the form of a mining allotment or a geological allotment...

4. Sections of land

4.1. Licenses for the right to use mineral resources are granted simultaneously with the right to use the corresponding plots of land. The acquisition of plots of land for temporary use or their confiscation (redemption) are carried out in keeping with land legislation of the Russian Federation and the republics of the Russian Federation and also legal acts of the krays, oblasts, autonomous entities...

5. The system of payments when mineral resources are used.

5.1. From the users of mineral resources... payments are collected, which include: payment for the right to use the mineral resources, deductions for reproduction of the mineral-raw material base, payment for the use of the water area and sections of the sea bottom.

Additionally, users of mineral resources pay taxes, excise taxes, and other fees and payments specified by legislation, including payment for land. For them one can establish a rebate from the payments for the right to use mineral resources, taking into account the depletion of the mineral resources...

5.6. Fees are collected for licenses for the right to use mineral resources...

6. Kinds of licenses

...6.2. A license for geological study of mineral resources certifies the right to conduct exploration and evaluate deposits of mineral resources and objects used for the construction and operation of underground structures not involved in the extraction of mineral resources.

A license for detailed study (prospecting) of deposits of mineral resources is not granted separately; the right to prospecting is envisioned in the license for the extraction of the mineral.

A license for a geological study of mineral resources grants the right to study only the kind (or kinds) of mineral resources indicated on the license, and does not give the holder a priority right to acquire a license for the right to extraction...

6.3. A license for extraction of a mineral resource grants the right to prospect and develop the deposits and also process the byproducts from ore extraction and processing productions related to it...

6.9. It is permitted to issue licenses which include several kinds of use of mineral resources (exploration, prospecting, and extraction of mineral resources...

7. Period of validity of licenses

7.1. Licenses are issued for geological study for a period of up to five years, for extraction of mineral resources and for purposes not related to extraction—up to 20 years; with a combination of geological study and extraction of mineral resources—up to 25 years...

8. Content of licenses:

A license must contain:

8.1. information about the user of the mineral resources who has received the license;

8.2. information about the purpose of the work involving the use of mineral resources;

8.3. an indication of the space limits of the section of mineral resources granted for use;

8.4. an indication of the boundaries of the land allotment granted for conducting work related to the use of mineral resources;

8.5. periods of validity of the license and deadline for the beginning of the work;

8.6. conditions related to payment collected with the use of mineral resources, plots of land, and water areas;

8.7. the agreed-upon level of extraction of mineral raw material and also an agreement for distribution of shares of it;

8.8. the agreement on rights to geological information obtained during the process of the use of the mineral resources;

8.9. conditions for the fulfillment of requirements established by legislation and standards (norms, rules) for protection of mineral resources and the environment and safe work;

8.10. conditions for extending the period of validity of the license;

8.11. the volumes and kinds of production and industrial waste water discharged into the earth's interior.

Extractive Metallurgy, Mining

A license for the right to use mineral resources registers the conditions and the form of contractual relations for the use of mineral resources, including the conditions of the concession, the agreement to divide up the products, and the contract for rendering services (with or without risk), and it can also be augmented by other conditions that do not contradict the law of the Russian Federation "On Mineral Resources" or the present statute.

9. Owners of licenses

9.1. Subjects of entrepreneurial activity may be owners of licenses, regardless of the form of ownership, including legal entities and citizens of other states (henceforth in the text—enterprises) unless otherwise stipulated by legislative acts of the Russian Federation. Only state enterprises may use mineral resources for the extraction of radioactive raw material...

10. The system of selecting applicants for a license

10.1. Licenses for the right to use mineral resources are granted through holding competitions and auctions...

10.3. With a competition system the winner is the applicant who satisfies the conditions of the competition and has been able to prove that the technical solutions he proposes are economically acceptable and correspond most fully to the requirements for protection of mineral resources and the environment...

10.4. With the auction system of issuing licenses the winner is the applicant who has offered the greatest payment for the right to use mineral resources...

11. The mechanism for issuing licenses

11.1. Enterprises wishing to obtain a license for the right to use mineral resources must apply to the State Committee for Geology of Russia or its territorial subdivisions...

11.2. ...Information about objects placed in competition or auction is published in official federal, republic, kray, oblast, and local press organs no later than three months, and for large objects—six months, before the date when they are to be held...

11.4. Enterprises applying for a license must, by the established deadline, submit to the organ issuing the licenses an application, which must contain:

- 1) information about the applicant enterprise, including the location of its main business activity and its economic relations with financial and production partners;
- 2) information about the leaders (or owners) of the enterprise that has submitted the application and the individuals who will represent this enterprise upon receipt of the license;

3) information about the financial capabilities of the applicant enterprise necessary for performing work related to the intended use of mineral resources, confirmed by financial organs;

4) information about the technical and technological capabilities of the enterprise and also other enterprises enlisted as subcontractors;

5) information about prior activity of the enterprise, including a list of countries in which it has conducted its activity in the last five years;

6) proposals from the applicant concerning the conditions for the use of mineral resources.

11.5. Applications submitted for participation in an auction go through an expert evaluation in the State Committee for Geology of Russia or its territorial subdivisions from the standpoint of the financial and technical competence of the applicant. The application is considered accepted after the applicant pays the license fee, of which he is notified in writing...

11.8. After the acceptance of the application for participation in the competition, the applicant for the license receives a packet of preliminary geological information concerning the section of mineral resources that interests him. The packet should contain a sufficient amount of geological, mining-technical, technological, and other information for doing technical-economic calculations.

On the basis of a study of the geological information the applicant for the license develops within the established time period and submits the basic technical and economic indicators for conducting the work involved in the intended use of the mineral resources.

11.9. The assessment of the correspondence of the technical and economic indicators developed by the applicants to the conditions of the competition is made by the expert commission and documented in a protocol.

The formation of expert commissions and the determination of the winners of the competition from among the applications... are done by the organ of representative power... and the State Committee for Geology of Russia and its territorial subdivisions...

20. The granting of licenses to enterprises using mineral resources until the present statute goes into force

20.1. All operating mining and other enterprises that use mineral resources, including those that have a mining allotment or have been granted the right to use mineral resources under another policy (including gold mining expeditions working in mining allotments of state enterprises) must within a month after the day the present statute goes into force submit an application to confirm its right to use mineral resources through obtaining a license...

Thermostable Magnets of Hysteretic Motor System

927D0133H Sverdlovsk FIZIKA METALLOV I METALLOVEDENIYE in Russian No 10, Oct 91 pp 148-153

[Article by Ye.V. Belozerov, N.M. Kleynerman, T.P. Lapina, L.M. Magat, V.V. Serikov, Ye.I. Teytel, Institute of Physics of Metals at the Urals Department of the USSR Academy of Sciences; UDC 669.15'25'26:537.622]

[Abstract] The use of plastic-deformable Fe-Co-Cr system alloys for making permanent magnets whose characteristics are comparable to those of alnico alloys and the shortcomings of traditional heat treatment methods which do not ensure the requisite thermal stability of the magnets are discussed; the possibility of improving the thermal stability of permanent magnets from the Fe-Co-Cr system alloy is investigated. The ingots for the study are smelted in an induction furnace in an argon atmosphere from pure burden materials and cast into metal molds, then forged at a 900-1,000°C temperature into a 20 mm dia. rod from which ring-shaped samples are made. The measurements are taken by a high-temperature vibratory magnetometer. X-ray structural analysis, nuclear gamma resonance studies, and an electron microscope examination (under a JEM-200CX) are conducted. The dependence of the temperature coefficient of the magnetizing field ensuring the necessary induction on the coercive force and heating temperature of the permanent magnet, the effect of the Co : Cr ratio on the temperature coefficient, the temperature dependence of magnetic moment and coercive force, hysteretic curves, and nuclear gamma resonance (YaGR) spectra of permanent magnets from the Kh23K15GaM alloy are plotted, and the hyperfine field distribution function in the samples is examined. Structural analyses make it possible to conclude that the

thermostabilizing low-temperature treatment leads to an additional decay of the alloy matrix and its individual nonequilibrium segments while the phase concentration difference increases due to a chromium migration. Figures 7; references 16: 11 Russian, 5 Western.

Effect of Magnetized Water on Dough Properties and Bread Quality

927D0148E Kishinev ELEKTRONNAYA OBRABOTKA MATERIALOV in Russian No 5 (161), Sep-Oct 91 pp 60-62

[Article by A.M. Ostapenkov, I.M. Mamatov, Kh.P. Sadinov, Samarkand Cooperative Institute of Central Union imeni V.V. Kuybyshev]

[Abstract] The effect of water magnetization on the activity of amylase and lipase is discussed and the effect of the magnetic field strength, the duration of the magnetic water treatment, and the water flow rate on the water magnetization efficiency is investigated. To this end, the rate of carbon dioxide production as a function of the dough temperature and fermentation duration is examined; the experimental results demonstrate that the volume of the dough kneaded with magnetized water increases rapidly at first; then, some 90 minutes later, the dough rate of growth becomes virtually identical regardless of whether it is kneaded with magnetized or regular tap water. This is attributed to the fact that the fermentation process is faster in leavened dough kneaded with magnetized water. The experiments also show that the acidity increases by an average of 19 percent in a dough prepared with magnetized water due to the flour's increased gas generating capacity. The dough acidity is summarized. Thus, the fermentation duration of the magnetized-water dough is shortened by 35-38 percent while the quality and taste of bread improve; it becomes less sticky and has higher organoleptic indices. Figures 1; tables 1; references 3.

NTIS
ATTN PROCESS 103
5285 PORT ROYAL RD
SPRINGFIELD VA

N2

22161

This is a U.S. Government publication. Its contents in no way represent the policies, views, or attitudes of the U.S. Government. Users of this publication may cite FBIS or JPRS provided they do so in a manner clearly identifying them as the secondary source.

Foreign Broadcast Information Service (FBIS) and Joint Publications Research Service (JPRS) publications contain political, military, economic, environmental, and sociological news, commentary, and other information, as well as scientific and technical data and reports. All information has been obtained from foreign radio and television broadcasts, news agency transmissions, newspapers, books, and periodicals. Items generally are processed from the first or best available sources. It should not be inferred that they have been disseminated only in the medium, in the language, or to the area indicated. Items from foreign language sources are translated; those from English-language sources are transcribed. Except for excluding certain diacritics, FBIS renders personal names and place-names in accordance with the romanization systems approved for U.S. Government publications by the U.S. Board of Geographic Names.

Headlines, editorial reports, and material enclosed in brackets [] are supplied by FBIS/JPRS. Processing indicators such as [Text] or [Excerpts] in the first line of each item indicate how the information was processed from the original. Unfamiliar names rendered phonetically are enclosed in parentheses. Words or names preceded by a question mark and enclosed in parentheses were not clear from the original source but have been supplied as appropriate to the context. Other unattributed parenthetical notes within the body of an item originate with the source. Times within items are as given by the source. Passages in boldface or italics are as published.

SUBSCRIPTION/PROCUREMENT INFORMATION

The FBIS DAILY REPORT contains current news and information and is published Monday through Friday in eight volumes: China, East Europe, Central Eurasia, East Asia, Near East & South Asia, Sub-Saharan Africa, Latin America, and West Europe. Supplements to the DAILY REPORTS may also be available periodically and will be distributed to regular DAILY REPORT subscribers. JPRS publications, which include approximately 50 regional, worldwide, and topical reports, generally contain less time-sensitive information and are published periodically.

Current DAILY REPORTS and JPRS publications are listed in *Government Reports Announcements* issued semimonthly by the National Technical Information Service (NTIS), 5285 Port Royal Road, Springfield, Virginia 22161 and the *Monthly Catalog of U.S. Government Publications* issued by the Superintendent of Documents, U.S. Government Printing Office, Washington, D.C. 20402.

The public may subscribe to either hardcover or microfiche versions of the DAILY REPORTS and JPRS publications through NTIS at the above address or by calling (703) 487-4630. Subscription rates will be

provided by NTIS upon request. Subscriptions are available outside the United States from NTIS or appointed foreign dealers. New subscribers should expect a 30-day delay in receipt of the first issue.

U.S. Government offices may obtain subscriptions to the DAILY REPORTS or JPRS publications (hardcover or microfiche) at no charge through their sponsoring organizations. For additional information or assistance, call FBIS, (202) 338-6735, or write to P.O. Box 2604, Washington, D.C. 20013. Department of Defense consumers are required to submit requests through appropriate command validation channels to DIA, RTS-2C, Washington, D.C. 20301. (Telephone: (202) 373-3771, Autovon: 243-3771.)

Back issues or single copies of the DAILY REPORTS and JPRS publications are not available. Both the DAILY REPORTS and the JPRS publications are on file for public reference at the Library of Congress and at many Federal Depository Libraries. Reference copies may also be seen at many public and university libraries throughout the United States.